Referee #2

Major Comments:

"As one of the most important absorbing aerosols in the atmosphere, black carbon (BC) does play crucial roles in regional and global climate change. Both fossil fuel combustion and biomass burning contribute significantly to atmospheric BC, but its emission attributions are still not fully understood and are of great uncertainty. This work aims to quantify the contributions from different factors to sources of global BC in the atmosphere and in deposition by conducting global transport model and comparing it with the observations. The strength of this work is comprehensive observational data in multiple typical regions across the world. However, the authors jump to the conclusion several times in the interpretation of gaps between observational data and model results, and some bias are not clearly presented or fully investigated. Thus, more in- depth analysis ought to be provided. Here are some issues that need to be addressed for further improving this work."

1 *"Section 2: The descriptions of simulation design and observations are far too simple. All the model configuration and simulations need to be introduced in detail. It is very confusing to understand EXP. A-D in Figure 4 without any introduction of these experiments in this part. And also, why these experiments are designed should be well documented."*

Response: Why we design the experiments are documented in Sect. 4.3. Since the some of the uncertainty experiments are based on the results of the standard simulation, it's hard to move the description of Exps. A-D to the model description part. We decided to leave the exp. description in Sect. 4.3.

2 *"As presented in Fig. 1-2, there does exist substantial gaps between model simulations and observational fbb in magnitude, seasonal variation, as well as spatial patterns. The authors generally describe the model bias and possible factors. However, more validation and detailed comparison may provide further in-depth information on model performance and uncertainties in related processes.*

2.1*. In addition to observed and GEOS-Chem simulated fraction of biomass burning of BC, information on the model performance on BC magnitude in different seasons may be helpful to understand the causes of the biases. Fig. S1 compared the Observed and GEOS-Chem simulated annual BC concentration but missed its seasonality and regional discrepancies. Since this work gathered carbon isotope analysis of BC at dozens of sites across the globe in different seasons, I do think detailed comparison and analysis on seasonal and regional bias of model simulation worth to be conducted."*

Response: Seasonal variations of BC concentration in different regions do help understand the model bias of BC concentration, but provide limited information on bias of BC sources, since BC concentration and f_{bb} have distinctively different seasonal

variations as we discussed in the manuscript in P6 L9-12. In addition, most of the seasonal observations of BC are publicly unavailable. We only have seasonal variations of BC from IMPROVE network in the United States (as discussed in Qi et al. (2017)) and in the Arctic. Sources of BC in the Arctic are discussed in detail in a separate manuscript (Qi and Wang, 2019 in review). Considering the limited sites (only two) with carbon isotope measurements, we think analyzing seasonal variations of BC concentration from IMPROVE measurements do not provide proper information for the source apportionment analysis.

2.2 *"As pointed out by the author, the bias in model results of fraction of biomass burning of BC can be greatly attributed to the lack of seasonality of existing fossil and biofuel combustion since that biomass burning emissions feature substantial temporal variations. To avoid the systematic bias caused by crude treatment of emission sources, monthly global emission inventory like EDGAR or HTAPv2 data or the monthly profile therein can be used as emission input of the model. "*

Response: We apply seasonal variations to domestic heating (Sect. 2). Other sectors, such as industry and transport, have little or no seasonal variations. We use daily emissions of GFED4 for open fire emissions (Sect. 2). We also revised some of the related analysis in Sect. 4.

2.3 *"Since BC is one of typical primary pollutants in the atmosphere, transport process is of great importance besides emission sources. The relatively coarse spatial resolution (4◦ latitude × 5◦ longitude) is not capable to capture some subtle meteorological conditions, which is vital for BC's transport and diffusion. Additionally, the coarse resolution make us to reconsider the representativeness of these observational sites, especially those near the complex terrain or mixed land cover. Applying fine spatial resolution in GEOS-Chem model may help reduce the bias of the model."*

Response: We added uncertainty analysis of model resolution in Sect. 4.3.5.

Specific comments:

3. *"Page 6, Line 2 and Line 19-20: Please list the reference here. Did the authors get this conclusion based on emission inventories or existing publications. Anyhow, this statement should be supported by data or references. "*

Response: Clarified.

4. *"Page 3,Line 8: change to "3 nm" "*

Response: Done.

5. *"Page 10,Line 1: "leaded" should be "led""*

Response: Done.

References

Qi, L., Li, Q., He, C., Wang, X., and Huang, J.: Effects of the Wegener–Bergeron–Findeisen process on global black carbon distribution, Atmospheric Chemistry and Physics, 17, 7459-7479, doi:10.5194/acp-17-7459-2017, 2017a.

Qi, L., and Wang, S.X.: Sources of black carbon in the atmosphere and in snow in the Arctic, Science of the Total Environment, 2019, in review.

Fossil fuel combustion and biomass burning sources of global black carbon from GEOS-Chem and carbon isotope measurements

Ling Qi[1] and Shuxiao Wang[1,2]

[1]State Key Joint Laboratory of Environment Simulation and Pollution Control, School of Environment, Tsinghua University, Beijing 100084, China
[2]State Environmental Protection Key Laboratory of Sources and Control of Air Pollution Complex, Beijing 100084, China

Correspondence to: Shuxiao Wang (shxwang@tsinghua.edu.cn)

Abstract. We identify sources (fossil fuel combustion versus biomass burning) of black carbon (BC) in the atmosphere and in deposition using a global 3D chemical transport model GEOS-Chem. We validate the simulated sources against carbon isotope measurements of BC around the globe and find that the model reproduces mean biomass burning contribution (f_{bb}, %) in various regions within a factor of 2 (except in Europe, where f_{bb} is underestimated by 63%). GEOS-Chem shows that contribution from biomass burning in the Northern Hemisphere (f_{bb}: 35±14%) is much less than that in the Southern Hemisphere (50±11%). The largest atmospheric f_{bb} is in Africa (64±20%). Comparable contributions from biomass burning and fossil fuel combustion are found in South (S.) Asia (53±10%), Southeast (SE.) Asia (53±11%), S. America (47±14%), S. Pacific (47±7%), Australia (53±14%) and the Antarctic (51±2%). f_{bb} is relatively small in East Asia (40±13%), Siberia (35±8%), the Arctic (33±6%), Canada (31±7%), the US (25±4%), and Europe (19±7%). Both observations and model results suggest that atmospheric f_{bb} is higher in summer (59–78%, vary with sub-regions) than in winter (28–32%) in the Arctic, while it is higher in winter (42–58%) and lower in summer (16–42%) over the Himalayan–Tibetan plateau. The seasonal variations of Atmospheric f_{bb} are relatively flat in North America, Europe, and Asia. We conducted four experiments to investigate the uncertainties associated with biofuel emissions, hygroscopicity of BC in fresh emissions, aging rate and size-resolved wet scavenging. We find that double biofuel emissions for domestic heating north of 45°N increases f_{bb} values in Europe in winter by ~30%, reducing the discrepancy between observed and modeled atmospheric f_{bb} from -63% to -54%. The remaining large negative discrepancy between model and observations suggests that the biofuel emissions are probably still underestimated at high latitudes. Increasing fraction of thickly coated hydrophilic BC from 20% to 70% in fresh biomass burning plumes increases the fraction of hydrophilic BC in biomass burning plumes by 0–20% (vary with seasons and regions), and thereby reduces atmospheric f_{bb} by up to 11%. Faster aging (4 hour *e*-folding time versus 1.15 days of *e*-folding time) of BC in biomass burning plumes reduces atmospheric f_{bb} by 7% (1– 14%, vary with seasons and regions), with the largest reduction in remote regions, such as the Arctic, the Antarctic and S. Pacific. Using size resolved scavenging accelerates scavenging of BC particles in both fossil fuel and biomass burning plumes, with a faster scavenging of BC in fossil fuel plumes. Thus, atmospheric f_{bb} increases in most regions by 1–14%. Overall, atmospheric f_{bb} is determined by f_{bb} in emissions mainly and by atmospheric processes, such as aging and scavenging, to a less extent. This confirms the

assumption that f_{bb} in local emissions determines atmospheric f_{bb} in previous studies, which compared measured atmospheric f_{bb} directly with local f_{bb} in bottom-up emission inventories.

1 Introduction

Black carbon (BC) in the atmosphere and deposited over snow and ice absorbs solar radiation, triggers positive feedbacks and exerts a positive radiative forcing on the global climate (IPCC, 2014). Estimates of BC radiative forcing span a large range (0.2–1 W m^{-2}, Bond et al., 2013; IPCC, 2014). One of the uncertainties lies in the orders of magnitude different predictions of BC vertical profiles around the globe, particularly in remote regions, by chemical transport and climate models (Samset et al., 2013; 2014). To reduce the uncertainty, in addition to the widely used BC concentration observations in the troposphere, at surface and in snow, observation-based source apportionment (fossil fuel versus biomass burning) of BC provides another dimension to constrain model simulations of BC distribution. The optical properties of BC from fossil fuel and biomass burning plumes are distinctively different (Bond et al., 2013), resulting in different radiative forcing from the two sources (Jacobson, 2010). Because of the relative short lifetime compared to greenhouse gases, accurate source apportionment of BC is important for short-term climate change mitigation.

Carbon isotope analysis is effective in distinguishing emissions from fossil fuel combustion (e.g. coal, oil and natural gas) and contemporary biomass burning (expressed as contribution from biomass burning, f_{bb}, %), because fossil emissions are ^{14}C free and biomass emissions have a characteristic $^{14}C/^{12}C$ ratio that is proportional to atmospheric carbon dioxide at the time of carbon fixation (Reddy et al., 2002). Combining $\delta^{13}C$ and $\Delta^{14}C$ measurements further differentiate the contribution from coal and liquid fossil fuel combustion (oil, gasoline and diesel, Andersson et al., 2015 and references therein). Fossil fuel combustion has an anthropogenic origin, including industrial use, domestic cooking and heating, and transport (Bond et al., 2007). Contemporary biomass burning can come from both anthropogenic and natural sources. The former includes mainly industrial and domestic burning of biofuels (fuelwood, charcoal, agricultural residues, and dung, Fernandes et al., 2007) and the latter involves open fires of forests, crops, grass, and peatlands (van der Werf et al., 2010). Carbon isotope measurements are widely used for source apportionment of BC in the atmosphere in South Asia (Gustafsson et al., 2009; Budhavant et al., 2015), East Asia (Chen et al., 2013; Andersson et al., 2015; Zhang et al., 2015; Li et al., 2016), Europe (Szidat et al., 2006; 2009; Zhang et al., 2012) and the Arctic (Barrett et al., 2015; Winiger et al., 2015; 2016; 2017), in snow over the Himalayan-Tibetan Plateau (Li et al., 2016) and in an Alpine ice core (Jenk et al., 2006).

Previous studies (Gustafsson et al., 2009; Chen et al., 2013; Li et al., 2016) compared carbon isotope measurements directly to f_{bb} of local bottom-up emission inventories. The assumption behind these studies is that the major controlling factor of f_{bb} in the atmosphere is local emissions. However, BC-containing particles in fossil fuel and biomass burning plumes have distinctively different mixing states and hygroscopicities (Moteki et al., 2007; Schwarz et al., 2008; Shiraiwa et al., 2007; Akagi et al., 2012), which might further affect BC scavenging in the two kinds of plumes and thus f_{bb} in the atmosphere and after deposition. Li et al. (2016) found smaller contribution from fossil fuel in snow than in air, suggesting that biomass

burning emissions are easier to deposit compared to fossil fuel combustion emissions. Possible factors affecting f_{bb} in the atmosphere and in deposition are mixing states and hygroscopicities in freshly emitted fossil fuel and biomass burning plumes, the consecutive aging rate and scavenging. However, as far as we are aware, no study has quantified the contribution of different factors to sources in terms of global BC in the atmosphere and in deposition.

In this study, we simulate sources of BC (fossil fuel combustion versus biomass burning) using a global 3D chemical transport model GEOS-Chem. We describe the model and the carbon isotope measurements in Sections 2 and 3, respectively. We evaluate the model simulation of f_{bb} in Section 4.1, analyze the spatial and temporal variations of f_{bb} in Section 4.2, evaluate the uncertainties associated with f_{bb} in BC emissions, BC mixing state and hycroscopicity in fresh emissions, aging rage and size-resolved scavenging in Section 4.3.

2 Model description

GEOS-Chem is a global chemical transport model driven with assimilated meteorological fields from the Goddard Earth Observing System (GEOS) of the NASA Global Modeling and Assimilation Office (Bey et al., 2001). We use GEOS-Chem v11.01 coupled with the TwO Moment Aerosol Section (TOMAS) microphysics scheme (Adams and Seinfeld, 2002). This is a state-of-the-art global model to simulate global distribution of BC (Wang et al., 2011; Qi et al., 2017 (a and c)). We use 15 size bins ranging from 3 nm to 10 μm with tracers for sulphate, sea salt, organic aerosols, BC, and dust (Pierce et al., 2007; Lee et al., 2009; D'Andrea et al., 2013; Kodros and Peirce, 2017). Modern-Era Retrospective analysis for Research and Applications, Version 2 (MERRA2) meterological data set are used to drive model simulation at 4° latitude × 5° longitude horizontal resolution and 47 vertical layers from the surface to 0.01 hPa. Global fossil fuel and biofuel combustion emissions of BC are from Bond et al. (2007) and Fernandes et al. (2007), respectively. We also include gas flaring emissions from Stohl et al. (2013). We replace BC emissions in Asia by Li et al. (2017). We apply seasonal variations for domestic heating emissions based on degree-day concept (Stohl et al., 2013; Qi et al., 2017c). We use daily open fire emissions from Global Fire Emissions Database version 4 (GFED4, Giglio et al., 2013) in this study. We assume 20% of the freshly emitted BC aerosols are thickly coated and are hydrophilic (Park et al., 2003). We assume hydrophobic BC is converted to hydrophilic with an *e*-folding time of 1.15 days (Park et al., 2005). Wet deposition follows Liu et al. (2001), with updates of below cloud scavenging efficiency and in-cloud scavenging in ice clouds in Wang et al. (2011) and updates of BC scavenging in mix-phase clouds in Qi et al. (2017a).

3 Observation data

Carbon isotope analysis of BC sources in the atmosphere is available at 65 sites across the globe in different seasons to our knowledge (Table S1 and Fig. S3). Generally, f_{bb} values are larger in remote regions (36±16% in South Asia, 33±14% in the Arctic and 39±17% over the Himalayan–Tibetan plateau) than those in urban regions (13±4% in North America), indicating

a larger contribution from biofuel and open fires in rural, developing and remote regions. In addition, f_{bb} values strongly depend on seasons (see detailed analysis in Sect. 4.2.1). Carbon isotope measurements of BC in snow are only available over the Tibetan Plateau from Li et al. (2016).

Isotope mass balance equation based on the $\Delta^{14}C$ ($^{14}C/^{12}C$) data was applied to apportion the relative contributions to atmospheric BC from biomass burning of modern carbon (f_{bb}) and fossil fuel combustion.

$$\Delta^{14}C = \Delta^{14}C_{bb} f_{bb} + \Delta^{14}C_{ff} (1 - f_{bb}) \quad (1)$$

Where $\Delta^{14}C$ is the measured radiocarbon content of the BC component and $\Delta^{14}C_{ff}$ is -1,000‰ by definition because fossil carbon is completely depleted in radiocarbon (Li et al., 2016). $\Delta^{14}C_{bb}$ end members used in this equation are usually between +70‰ and +225‰, depending on the type and age of the burned biomass (Winiger et al., 2015; Barrett et al., 2015; Li et al, 2016). The former value corresponds to freshly produced biomass, such as crop and grass. The latter value reflects the burn of wood, which has accumulated over the decades-to-century-long life span. Different choice of the $\Delta^{14}C_{bb}$ end member is one of the uncertainties associated with this source apportionment method. Uncertainty of ±25‰ translates to < 5% in the resulting f_{bb} estimate (Winiger et al., 2016). Another uncertainty stems from the method of isolating BC from total carbon in sampled particles (Zhang et al., 2012). They found that the isolation method prior to thermal treatments, thermal-optical methods, and the heating protocols are important to the isolation of BC and organic carbon and the following isotope analysis. They found that different protocols of thermal-optical method lead to ~ 30% difference of estimated f_{bb} values.

4 Results and Discussions

GEOS-Chem captures the probability density function (PDF) of annual BC concentrations at sites in the US, Europe, China and the Arctic (see site description in Qi et al., 2017(b)) but overestimates the frequency of low BC concentrations (Fig. 1S (a)). About 30% of the simulated annual BC concentration in air is underestimated by a factor of 2 (Fig. 1S (b)). The model reproduces the PDF of BC concentration in snow preferably (correlation coefficient r = 0.98, Fig. 2S (a)). The simulated median BC concentrations in snow in various regions agree with observations within a factor of 2, except in region NC_Northeast Border (Fig. 2S (b)), where the model overestimates the observed BC concentration in snow by a factor of 3 due to the overestimate of local emissions in that region (Qi et al., 2017b).

4.1 Contribution of biomass burning to BC in various regions

GEOS-Chem simulated mean atmospheric f_{bb} in each region agrees with observations within a factor of 2, except in Europe, where f_{bb} is underestimated by 63% (Fig.1 (a)). The low bias of f_{bb} in Europe occurs in non-summer seasons (observation: 45%, model: 13%), which is partly due to the underestimate of biofuel combustion for domestic heating by Fernandes et al. (2007) in most of the European regions during cold seasons (Herich et al., 2011). In South (S.) Asia, mean atmospheric f_{bb} is

overestimated by 50%, mostly from the 90% overestimate of f_{bb} at Delhi (observation: 28%, model: 52%). At this site, atmospheric f_{bb} in spring and summer are overestimated by 100% and 200%, respectively. In North America, the model overestimates f_{bb} at Salt Lake City (SLC) and Mexican City by a factor of 2. Possible reasons for the overestimate are explained in Sect. 4.2.1. In the Arctic and East (E.) Asia, the model reproduces the observed f_{bb} values within 3% and 7%, respectively. In addition, GEOS-Chem underestimates the large variations of f_{bb} values (horizontal lines in Fig. 1 (a)) in every region (except in the Arctic), due to the coarse horizontal and vertical resolutions.

Over the Himalayan–Tibetan plateau, observations show that biomass burning dominates BC deposited in snow (64%), but its contribution in the atmosphere is much less (39%, Li et al., 2016). GEOS-Chem reproduces the average f_{bb} in snow (model: 63%) but overpredicts the average atmospheric f_{bb} (model: 62%) by 56%. GEOS-Chem simulated f_{bb} values of BC deposition in snow at all sites over the Himalayan–Tibetan plateau agree with observations within 40% during both monsoon (June–August) and non-monsoon seasons (Fig. 1 (b)), suggesting that the model captures the spatial and temporal variations of f_{bb} in BC deposition in this region. The overestimate of the atmospheric f_{bb} is mainly from 130% overestimate of f_{bb} during monsoon season (observation: 29%, model: 67%). Possible reasons for the overestimate are discussed in Sect. 4.2.1.

4.2 Temporal and spatial variations of f_{bb} in different regions

4.2.1 Temporal variation of f_{bb}

In the Arctic at Abisko, observed f_{bb} ranges from fall and wintertime low of 31% to summer high of 59% (Fig. 2(a)), due to the large contribution from open fires in Europe in summer (Winiger et al., 2016). The model also shows a peak of f_{bb} in summer, but the seasonal variation is relatively flat (from 23% in winter to 27% in summer). We attribute the discrepancy to two reasons. First, f_{bb} values of emissions at the site lack seasonal variations, as shown in Fig.2(a). Second, the coarse resolution does not solve the vortex structure of the low-pressure and frontal systems, which is important for poleward transport of BC (Ma et al., 2014; Sato et al., 2016). At Barrow (Fig. 2 (b)), observed f_{bb} show two peaks in summer (34%) and winter (37%), while modeled f_{bb} shows a single strong peak in summer (78%). In summer, the magnitude and variations of f_{bb} in the atmosphere is similar to that of f_{bb} in local emissions, suggesting that the atmospheric f_{bb} is largely determined by local emissions. The 129% overestimate of f_{bb} is largely due to the overestimate of local open burning emissions. In spring, fall and winter, the modeled atmospheric f_{bb} values are much larger than the f_{bb} of local emissions, indicating a large contribution from long-range transport.

In contrast to the seasonal cycles of f_{bb} at sites in the Arctic, at Bode (Fig. 2(c)) over the Himalayan–Tibetan Plateau, f_{bb} values are the lowest in summer (observation: 17%) and highest in winter (observation: 42%, Li et al., 2016). Similar trend is observed at Lumbini (Fig. 2(d)), only with smaller amplitude (summer low: 42%, spring high: 58%, Li et al., 2016). The lower f_{bb} in summer is because of several reasons. First, less biofuel is consumed for domestic heating in warmer seasons (Li et al., 2016). Second, the region is barely affected by open fires. Third, biomass-sourced BC is removed more efficiently by the frequent precipitation in summer both over the Himalayan–Tibetan plateau and over the surrounding source regions, such

as India and East Asia (Li et al., 2016). The GEOS-Chem simulated atmospheric f_{bb} of BC at all sites over the Himalayan–Tibetan plateau (results for Bode and Lumbini are shown in Fig. 2 (c) and (d) and the others are not) have weak or no seasonal variations. In addition, the model does not capture the observed increasing trend of f_{bb} along the Mustang valley and Langtang valley. Possible reasons for the discrepancies are several folds. First, the f_{bb} values of local emissions have no seasonal variations, as shown in Fig. 2 (c) and (d). Second, it is conceivable that the coarse model resolution of global models does not reproduce the complex topography and transport pathways of BC over the Himalayan–Tibetan plateau (He et al., 2014). However, the mean modeled atmospheric f_{bb} generally agrees with observations (within 60%) and the modeled atmospheric f_{bb} generally follows the f_{bb} of local emissions across the whole plateau. These comparisons suggest that the atmospheric f_{bb} over the Himalayan–Tibetan plateau is largely determined by f_{bb} in emissions in the region.

At sites SLC (North America, Fig. 2(e)), Tokyo (East Asia, Fig. 2(f)), MCOH and SINH (South Asia, Fig. 2(g) and (h)), no big differences of f_{bb} among seasons were observed (SLC: 8–13%; Tokyo: 33–41%; MCOH: 52–53%; SINH: 48–56%). However, BC concentrations show strong seasonal variations at the four sites, with high loadings in winter and low loadings in summer (Mouteva et al., 2017; Yamamoto et al., 2007; Budhavant et al., 2015). At SLC, the most significant local sources of $PM_{2.5}$ particles are mobile emissions, which are relatively stable through the whole year (Mouteva et al., 2017). The second most important source is non-mobile sources with solid burning, mostly wood burning, which is not allowed to use when air quality forecasts predict an inversion period (Mouteva et al., 2017). This restriction limits the extra use of solid fuels in winter, and thus limited their effects on BC concentrations and f_{bb} in the atmosphere. So the higher concentration of BC in winter in SLC is largely determined by the low boundary layer height (Mouteva et al., 2017). The model overestimates f_{bb} at SLC in all seasons by a factor of 2–4 (Fig. 2(e)). As described in Mouteva et al. (2017), the observations were in urban environment with strong influence from local emissions. However, modeled f_{bb} in the atmosphere is much higher than the f_{bb} values of local emissions based on emission inventories in this study (Sect. 2), suggesting that the modeled atmospheric f_{bb} at the site is largely affected by the surrounding regions. The misrepresentation of source region (local versus regional) is probably one reason of the large bias of modeled f_{bb} against observations. At site Tokyo, East Asia, the model reproduces both the magnitude and the seasonal variations of observed f_{bb}. The much lower f_{bb} value in emissions than in the atmosphere also indicates a regional effect. In South Asia, GEOS-Chem reproduces the similar observed high f_{bb} values at MOCH (summer: 52%; winter: 53%) and SINH (summer: 48; winter: 56%) within 30%. However, reasons for the high f_{bb} values at the two sites are different. Since there are no local emissions at MCOH, f_{bb} at the site is largely affected by long-range transport. In contrast, f_{bb} in the atmosphere follows f_{bb} in local emissions at SINH, suggesting that the atmospheric f_{bb} at the site is mostly affected by local emissions. At MCOH the high f_{bb} is probably from the large f_{bb} in the outflow of Africa, while at SINH local burning of agricultural crop residues are the major sources (Budhavant et al., 2015).

4.2.2 Spatial variation of modeled f_{bb}

GEOS-Chem suggests that the Southern Hemisphere has a higher contribution from biomass burning both for BC in surface air (50±11%) and in deposition (53±10%, Fig. 3 (a) and (b)). The high f_{bb} in S. America and Australia are largely from active

open fires (accounting for 48% and 81% of the total biomass burning contributions, respectively), while in Africa biofuel consumption is the major biomass burning source (model: 64±20%, Fig. 3 (c) and (d)). Because of the strong seasonal variations of open fire emissions, the highest f_{bb} in Africa, S. America, S. Pacific, Australia and the Antarctic usually occur during September to November (58–71%), and the lowest values are in March–May (32–56%, Fig. S4).

In the Northern Hemisphere, the largest f_{bb} of both BC in the atmosphere (93±5%) and in deposition (92±6%) are in North Congo, where biomass burning contribution dominates over fossil fuel emissions. South Asia also shows large f_{bb} (54% for BC in air and in deposition) due to large biofuel consumption. In other regions, such as Europe, Canada, the US, Siberia and the Arctic, fossil fuel contribution (65–80%) is much larger than biomass burning. f_{bb} of BC in air and in deposition in different regions have different seasonal variations (Figs. S4–S5). Atmospheric f_{bb} in Canada, Siberia, the Arctic and the Antarctic have the strongest seasonal variations with a peak in summer (49–70%) because of the large fraction of open fire emissions (Fig. S6–S7). In the US, South Europe, East Asia and South Asia, seasonal variation of f_{bb} is relatively flat, which is also shown by observations at a few sites (Fig. 2).

4.3 Uncertainty analysis

Atmospheric f_{bb} is determined not only by emissions (fossil fuel combustion versus biomass burning), but also by atmospheric processes that affect the deposition during transport. We investigate the uncertainties associated with biofuel emissions, f_{bb} in fresh emissions, BC aging rate and size-resolved scavenging. We used relative change (r, %) to describe the change of f_{bb} in each experiment (Exp.) relative to the standard simulation.

$$r = ([f_{bb}]_{Exp.} - [f_{bb}]_{Std.})/[f_{bb}]_{Std} \quad (2)$$

where r is the relative change, $[f_{bb}]_{Exp.}$ is f_{bb} in each experiment and $[f_{bb}]_{Std}$ is the f_{bb} in the standard simulation in each region.

4.3.1 Uncertainty associated with biofuel emissions

Biofuel emission estimates are associated with large uncertainties (Fernandes et al., 2007). Source apportionment of BC in Europe based on multi-wavelength aethalometer measurements showed that f_{bb} in winter (24–33%) is much higher than that in summer (2–10%), suggesting that wood burning for domestic heating increases the f_{bb} value in the atmosphere in winter significantly (Herich et al., 2011). In addition, Winiger et al. (2017) analyzed f_{bb} based on carbon isotope measurements at Tiksi in Russia and suggested that domestic (~60% of which is from biomass burning) accounted for 35% of BC at the site, following transport (38%). We find that during cold season mean f_{bb} values in Europe and the Arctic (most sites are north of 45°N, Table S1) are underestimated by 68% and 50% in the standard simulation, probably due to the underestimate of domestic heating in winter. However, in East Asia (all sites are south of 45°N), mean f_{bb} in winter is overestimated by 22%. Thus, we doubled biofuel emissions from domestic heating north of 45°N during cold seasons in Experiment (Exp.) A to

investigate the uncertainty associated with biofuel emissions. It is conceivable that the largest effects occur in the Northern four regions, including Europe, Siberia, Canada and the Arctic. As a result, f_{bb} values increase by ~30% in Europe, Siberia and the Arctic and by 15% in Canada in winter, larger than that in spring and fall (4–13%, Fig. 4). Consequently, the low bias of f_{bb} in Europe is reduced from -63% to -54%. This improvement suggests that the biofuel emissions at high latitudes in the Northern Hemisphere are probably too low in current bottom-up BC emission inventories, supporting previous estimates (Herich et al., 2011).

4.3.2 Uncertainty associated with hygroscopicity of BC in freshly emitted biomass burning plumes

Recent measurements find that in freshly emitted fossil fuel plumes the fraction of thickly coated hydrophilic BC is ~10% (Moteki et al., 2007; Schwarz et al., 2008; Shiraiwa et al., 2007), while in biomass burning plumes the fraction reaches up to 70% (Schwarz et al., 2008; Akagi et al., 2012). The higher hygroscopicity of BC in freshly emitted biomass burning plumes enhances the subsequent wet scavenging rate and thereby reduces f_{bb} in the atmosphere. In the standard simulation, we assume 20% of freshly emitted BC particles are hydrophilic. We investigate the effects of the initial hygroscopicity of BC in fresh emissions on atmospheric f_{bb} of BC in Exp. B by assuming 70% of freshly emitted BC particles from biomass burning are thickly coated and hydrophilic. The resulting fraction of hydrophilic BC in biomass burning plumes in the 12 regions increase by 0–20% (vary with seasons and regions), lowering f_{bb} in the atmosphere by up to 11% in Canada in summer. The largest reduction of f_{bb} shows in June–August (-7% averaged for all regions, Fig. 4), when open fires are frequent and active globally (Giglio et al., 2013; van der Werf et al., 2010). During this time, the largest reductions are in Canada (-11%) and Siberia (-10%), where the fraction of hydrophilic BC in biomass burning plumes increases by a large fraction (11–13%). In S. Pacific, the reduction of f_{bb} is large (-10%) as well, because large precipitation (28 kg m^{-2} mon^{-1}) over this region removes more biomass burning BC particles in the outflow of S. America. During September–November, the relative reduction of f_{bb} in the Northern Hemisphere (-6%) is much larger than that in the Southern Hemisphere (-1%), because f_{bb} values in the Southern Hemisphere are too large (Fig. S5). The changes of f_{bb} values in other seasons in all regions are marginal.

4.3.3 Uncertainty associated with BC aging time

Mixing with organic and inorganic particles with larger hygroscopicity, BC particles become more hydrophilic during aging process (Bond et al., 2013). It is assumed that BC particles are converted from hydrophobic to hydrophilic with an *e*-folding time of 1.15 days after emission in the standard simulation (Park et al., 2005). However, observations showed that the fraction of thickly coated hydrophilic BC in urban fossil fuel plumes increases linearly with plume age (0.5–2.3% h^{-1}, Moteki et al., 2007; Shiraiwa et al., 2007; Subramanian et al., 2010; McMeeking et al., 2011), while BC aging follows a logarithmic trend with an *e*-folding time of 4 hours in biomass burning plumes (Akagi et al., 2012). The aging rates differ among plumes because of different BC sizes, co-emitted hygroscopic materials and oxidation capacities of the plumes (Bond et al., 2013). Thus, in Exp. C, we assume fossil fuel combustion generated BC ages linearly with a rate of 1% h^{-1}, while BC from biomass burning plumes ages with an *e*-folding time of 4 hours. This means that the fossil fuel plumes age slower than the standard

simulation and be scavenged slower, while the biomass burning plumes age much faster and are removed from the atmosphere faster in precipitation. This aging scheme leads to a 0–24% increase of fraction of hydrophilic BC in the atmosphere, which reduces f_{bb} by up to -14%. The largest reduction of f_{bb} is in S. Pacific in fall (MAM) and summer (DJF) in the Southern Hemisphere, followed by the Antarctic (-12%) during MAM and the Arctic (-11%) during SON. The reduction of f_{bb} is larger in remote regions and smaller in source regions, because it takes time for the different aging rates in fossil fuel and biomass burning plumes to affect the hygroscopicities of BC in the two plumes and the subsequent aging rates.

4.3.4 Uncertainty associated with size resolved scavenging

BC particles emitted from biomass burning plumes are usually larger in size and thicker in coating thickness (Schwarz et al., 2008; Sahu et al., 2012), suggesting an easier removal from the atmosphere. For example, observations (Schwarz et al., 2008; Sahu et al., 2012) showed that the mass median diameter of BC particles in biomass burning plumes is 193 nm with a coating thickness of 65 nm, while in fossil fuel plumes, the mass median diameter and coating thickness are 175 nm and 20 nm. In addition, because of the different coating materials, hygroscopicities of BC-containing particles in the two kinds of plumes are different as well. The coating materials of BC in urban plumes are dominated by sulfate and followed by nitrate and primary and secondary organics (Shiraiwa et al., 2007), while in biomass burning plumes, the major coating materials are organics (Sahu et al., 2012). For ambient air, characteristic κ values of organics and inorganics are 0.1 (0.01–0.5) and 0.7 (0.5–1.4, Petters and Kreidenweis, 2007; Gunthe et al., 2011 and references therein). Higher hygroscopicity of BC in fossil fuel plumes suggests that they are easier to be activated and serve as CCN compared to BC particles in biomass burning plumes. The higher hygroscopicity and smaller size of BC particles in fossil fuel plumes have opposite effect on their removal rate. Thus, we investigate the total effects of size-resolved scavenging in Exp. D. we use the TOMAS microphysics scheme to process the aging and wet scavenging of BC with different sizes from fossil fuel combustion and biomass burning. The mass median diameters of fossil fuel and biomass burning BC particles are assumed to be 160 nm and 200 nm, respectively. Size resolved coagulation, condensation, nucleation and cloud processing are implemented. Coating materials included are sulfate, nitrate, sea-salt, organics and mineral dust. The size-resolved aging and scavenging scheme leads to a larger increase of fraction of hydrophilic BC in fossil fuel plumes (by 16% (0–31%, vary with regions)) than in biomass burning plumes (by 12% (0–23%)). This increase in both fossil fuel and biomass burning plumes suggest that BC particles are removed faster in the size-resolved simulation than in the standard simulation with a bulk removal parameterization. The larger increase of the fraction of hydrophilic BC in fossil fuel plumes means that BC in fossil fuel plumes are removed faster than those in biomass burning plumes in the size-resolved simulation. This is probably because the total effect of higher hygroscopicity of coating materials and smaller size of BC in fossil fuel plumes is enhancing their removal. Thus atmospheric f_{bb} increases in most regions during MAM (by 1–14%), SON (by 0–7%) and DJF (by 1–12%). The most noticeable characteristics is that the increase of f_{bb} in Northern Hemisphere is larger than those in Southern Hemisphere, due to the large fraction of fossil fuel emissions in the Northern Hemisphere.

4.3.5 Uncertainty associated with model resolution

Finer model resolution is capable to reproduce small-scale meteorological conditions, which is critical to BC transport (Sato et al., 2016). We use horizontal resolution of 4° lat × 5° lon in the standard simulation and Exps. A–D, because the size-resolved microphysical scheme TOMAS in Exp. D is computationally expensive. We investigate the uncertainty associated with model resolution in Exp. E by using a finer horizontal resolution of 2° lat × 2.5° lon (Fig. 4). We find that relative to the standard simulation, f_{bb} in Exp. E changes by -5%–5% in the 13 regions in all seasons. In most regions, the absolute change is smaller than or equal to the change in Exp. A–D, except in mid-latitude and tropical regions in Exp. A. Averaged in the whole globe, the relative change of f_{bb} to the standard simulation is -1%.

4.3.6 Other uncertainties

Carbon isotope measurements of BC sources are associated with large uncertainties. Thermal-optical protocol used for the carbon isotope measurements of BC produce ~30% difference of observed f_{bb} values (Zhang et al., 2012), which is equal or larger than the uncertainties of modeled f_{bb} associated with biofuel emissions North of 45°N, aging rate and wet scavenging discussed in Sect. 4.3.1-4.3.4. The comparison of the two sets of data in Sect. 4.1 and 4.2 are within similar uncertainty range. In addition, we do not have carbon isotope measurements in the Southern Hemisphere to constrain the model results. Our analysis in this study is based only on model results.

In addition to the biofuel emissions discussed in Sect 4.3.1, open fire emissions, particularly in the boreal regions, are associated with large uncertainties (Randerson et al., 2012). Konovalov et al. (2018) found that open burning emissions of Siberian fires during May to September from GFED4 is possibly underestimated by a factor of 2 constrained by satellite observations of the aerosol absorption optical depth and the aerosol extinction optical depth. However, we find that during the same season, mean atmospheric f_{bb} at Tiksi in Russia is overestimated by 88%, indicating that open burning emissions in this region from GFED4 are possibly overestimated. This contradiction suggests that further studies are needed to better constrain the open burning emissions in boreal regions. In addition, the global fossil fuel (Bond et al., 2007) and biofuel emission inventory (Fernandes et al., 2007) used in this study are for year 2000 and the emissions in Asia (Li et al., 2017) are for year 2010. We estimated the f_{bb} from 2007 to 2013 using these constant inventories and varying open burning emissions from GFED4. The lack of inter-annual variations of BC fossil fuel and biofuel emissions also produces uncertainties, but it is difficult to quantify based on current knowledge.

5 Conclusions

This study sought to understand the relative contribution of fossil fuel combustion and biomass burning to global BC. We used GEOS-Chem (version 11-01-01) driven by MERRA2 assimilated meteorological fields to simulate BC concentration from fossil fuel and biomass burning. The source apportionment results were expressed as the fraction of BC from biomass

burning (f_{bb}). Simulated f_{bb} was validated against carbon isotope measurements of BC in the atmosphere at 65 stations across the Northern Hemisphere and 11 snow samples over the Himalayan–Tibetan plateau. We also investigated the uncertainties of f_{bb} associated with biofuel emissions, fraction of hydrophilic BC in fresh emissions, aging time and size-resolved scavenging.

The model reproduced the mean observed atmospheric f_{bb} in various regions and in snow over the Himalayan–Tibetan plateau within a factor of 2. Generally, values of atmospheric f_{bb} were larger in remote regions (33±14% in the Arctic, 39±17% over the Himalayan–Tibetan plateau and 36±16% in South Asia) than those in urban regions (13±4% in North America), indicating a larger contribution from biofuel and open burning sources in rural, developing and remote regions. f_{bb} was higher in summer (59–78%, vary with regions) than in winter (28–32%, vary with regions)) in the Arctic, while it was higher in winter (42–58%, vary with regions)) and lower in summer (16–42%, vary with regions)) over the Himalayan–Tibetan plateau. The simulated amplitudes of the seasonal variations were much smaller in the two regions. The seasonal variation was observed to be relatively flat in North America, East and South Asia. The simulated monthly mean f_{bb} in these regions agree with observations by -45–275%. The Southern Hemisphere had a higher atmospheric f_{bb} than the Northern Hemisphere (SH: 50±11%, NH: 35±14%) due to the large fraction of open burning emissions in S. America and Australia and large fraction of biofuel consumption in Africa. In the Northern Hemisphere, the highest f_{bb} was in S. Asia (54±10%), followed by E. Asia (41±13%), due to large biofuel consumption. In other regions, such as Europe, Canada, the US, Siberia and the Arctic, f_{bb} values are small (20–35%, vary with regions)).

Simulated f_{bb} was associated with uncertainties from all processes, including emissions, aging and deposition processes. We found that doubled biofuel emissions used for domestic heating north of 45°N resulted in a ~30% increase of f_{bb} in Europe, Siberia and the Arctic and a 15% increase in Canada in winter. This increase reduced the discrepancy of f_{bb} against observations from -63% to -54% in Europe, suggesting that the biofuel emissions at high latitudes were underestimated by the bottom-up emission inventories. Using a higher fraction of hydrophilic BC in fresh biomass burning plumes (uncertainty simulation: 70%, standard simulation: 20%) resulted in a reduction of f_{bb} in summer by -2 – -11%, with the largest reduction in Canada and Siberia, where open fires were frequent. In the standard simulation, it was assumed that BC in both fossil fuel and biomass burning plumes aged following an *e*-folding time of 1.15 days. In the uncertainty simulation, we used a 4 hour *e*-folding life time for BC in biomass burning plumes and a linear aging rate of 1% for BC in fossil fuel plumes. This led to a reduction of f_{bb} up to -14% in the atmosphere. The largest reduction was in S. Pacific in fall (MAM) and summer (DJF) in the Southern Hemisphere. The reductions in the Antarctic (-12%) and the Arctic (-11%) were also large in fall when there were large open fires in the Southern Hemisphere and at high latitudes in the Northern Hemisphere. Size-resolved aging and scavenging scheme led to a larger increase of fraction of hydrophilic BC in fossil fuel plumes (by 16% (0–31%)) than in biomass burning plumes (by 12% (0–23%)). Thus atmospheric f_{bb} increased in most regions during MAM (by 1–14%), SON (by 0–7%) and DJF (by 1–12%). Using finer model resolution produced -5%–5% relative change of atmospheric f_{bb} in the various regions, equal or smaller than the change caused by atmospheric processes.

This study showed that local emissions had a larger effect on atmospheric f_{bb} than other atmospheric processes. As discussed in Sect. 1, most previous studies compared measured atmospheric f_{bb} directly with f_{bb} in local emissions. We confirmed this assumption, but suggested considering the uncertainties associated with aging and scavenging (up to 14%). In addition, ~30% difference of isotope-based measurements of f_{bb} caused by the thermal-optical protocols in measuring BC should also be considered.

This study has important implications for estimating radiative forcing of global BC. Previous studies (Healy et al., 2015 and references therein) showed that BC-containing particles in open fires had no optical lensing effect. Considering the large contribution from biomass burning in S. Asia, SE. Asia and in the Southern Hemisphere as suggested in this study, the inclusion of lensing-related absorption enhancement in climate models for BC from both fossil fuel combustion and biomass burning sources may lead to an overestimate of the radiative forcing of global BC. Measurements of the optical properties of BC particles from different sources (fossil fuel versus biomass burning) in different regions are needed to better constrain its radiative forcing.

Author contribution

Ling Qi and Shuxiao Wang designed the experiments. Ling Qi performed the simulations. Ling Qi prepared the manuscript with contributions from Shuxiao Wang.

Acknowledgments

This work was supported by the National Natural Science Foundation of China (21806088 and 21625701), Key Projects of National Key Research and Development Program of the Ministry of Science and Technology of China (No.2017YFC0213005 and 2018YFC0213805),) and National research program for key issues in air pollution control (DQGG0101 and DQGG0301). We thank the two reviewers for their constructive comments on the manuscript.

References

Adams, P. J., and Seinfeld, J. H.: Predicting global aerosol size distributions in general circulation models, Journal of Geophysical Research: Atmospheres, 107(D19), 4370-4392, doi:10.1029/2001JD001010, 2002.

Akagi, S. K., Craven, J. S., Taylor, J. W., McMeeking, G. R., Yokelson, R. J., Burling, I. R., Urbanski, S. P., Wold, C. E., Seinfeld, J. H., Coe, H., Alvarado, M. J., and Weise, D. R.: Evolution of trace gases and particles emitted by a chaparral fire in California, Atmospheric Chemistry and Physics, 12, 1397-1421, doi:10.5194/acp-12-1397-2012, 2012.

Andersson, A., Deng, J., Du, K., Zheng, M., Yan, C., Skold, M., and Gustafsson, O.: Regionally-varying combustion sources of the January 2013 severe haze events over eastern China, Environ Sci Technol, 49, 2038-2043, doi:10.1021/es503855e, 2015.

Barrett, T. E., Robinson, E. M., Usenko, S., and Sheesley, R. J.: Source Contributions to Wintertime Elemental and Organic Carbon in the Western Arctic Based on Radiocarbon and Tracer Apportionment, Environ Sci Technol, 49, 11631-11639, doi:10.1021/acs.est.5b03081, 2015.

Bey, I., D. J. Jacob, R. M. Yantosca, J. A. Logan, B. Field, A. M. Fiore, Q. Li, H. Liu, L. J. Mickley, and M. Schultz, Global modeling of tropospheric chemistry with assimilated meteorology: Model description and evaluation, Journal of Geophysical Research, 106, 23073-23095, https://doi.org/10.1029/2001JD000807, 2001.

Bikkina, S., Andersson, A., Kirillova, E. N., Holmstrand, H., Tiwari, S., Srivastava, A. K., Bisht, D. S., and Gustafsson, Ö.: Air quality in megacity Delhi affected by countryside biomass burning, Nature Sustainability, 2, 200-205, doi:10.1038/s41893-019-0219-0, 2019.

Bond, T. C., Bhardwaj, E., Dong, R., Jogani, R., Jung, S., Roden, C., Streets, D. G., and Trautmann, N. M.: Historical emissions of black and organic carbon aerosol from energy-related combustion, 1850-2000, Global Biogeochemical Cycles, 21, GB2018, doi:10.1029/2006gb002840, 2007.

Bond, T. C., Doherty, S. J., Fahey, D. W., Forster, P. M., Berntsen, T., DeAngelo, B. J., Flanner, M. G., Ghan, S., Kärcher, B., Koch, D., Kinne, S., Kondo, Y., Quinn, P. K., Sarofim, M. C., Schultz, M. G., Schulz, M., Venkataraman, C., Zhang, H., Zhang, S., Bellouin, N., Guttikunda, S. K., Hopke, P. K., Jacobson, M. Z., Kaiser, J. W., Klimont, Z., Lohmann, U., Schwarz, J. P., Shindell, D., Storelvmo, T., Warren, S. G., and Zender, C. S.: Bounding the role of black carbon in the climate system: A scientific assessment, Journal of Geophysical Research: Atmospheres, 118, 5380-5552, doi:10.1002/jgrd.50171, 2013.

Budhavant, K., Andersson, A., Bosch, C., Kruså, M., Kirillova, E. N., Sheesley, R. J., Safai, P. D., Rao, P. S. P., and Gustafsson, Ö.: Radiocarbon-based source apportionment of elemental carbon aerosols at two South Asian receptor observatories over a full annual cycle, Environmental Research Letters, 10, 064004, doi:10.1088/1748-9326/10/6/064004, 2015.

Chen, B., Andersson, A., Lee, M., Kirillova, E. N., Xiao, Q., Krusa, M., Shi, M., Hu, K., Lu, Z., Streets, D. G., Du, K., and Gustafsson, O.: Source forensics of black carbon aerosols from China, Environ Sci Technol, 47, 9102-9108, doi:10.1021/es401599r, 2013.

D'Andrea, S., Häkkinen, S., Westervelt, D., Kuang, C., Levin, E., Kanawade, V., Leaitch, W., Spracklen, D., Riipinen, I., and Pierce, J.: Understanding global secondary organic aerosol amount and size-resolved condensational behavior, Atmospheric Chemistry and Physics, 13(22), 11519-11534, doi: 10.5194/acp-13-11519-2013, 2013.

Fernandes, S. D., Trautmann, N. M., Streets, D. G., Roden, C. A., and Bond, T. C.: Global biofuel use, 1850-2000, Global Biogeochemical Cycles, 21(2), GB2019, doi:10.1029/2006gb002836, 2007.

Giglio, L., Randerson, J. T., and van der Werf, G. R.: Analysis of daily, monthly, and annual burned area using the fourth-generation global fire emissions database (GFED4), Journal of Geophysical Research: Biogeosciences, 118(1), 317-328, doi:10.1002/jgrg.20042, 2013.

Gunthe, S. S., Rose, D., Su, H., Garland, R. M., Achtert, P., Nowak, A., Wiedensohler, A., Kuwata, M., Takegawa, N., Kondo, Y., Hu, M., Shao, M., Zhu, T., Andreae, M. O., and Pöschl, U.: Cloud condensation nuclei (CCN) from fresh and aged air pollution in the megacity region of Beijing, Atmospheric Chemistry and Physics, 11, 11023-11039, doi:10.5194/acp-11-11023-2011, 2011.

Gustafsson, Ö., Kruså, M., Zencak, Z., Sheesley, R. J., Granat, L., Engström, E., Praveen, P., Rao, P., Leck, C., and Rodhe, H.: Brown clouds over South Asia: biomass or fossil fuel combustion?, Science, 323, 495-498, doi: 10.1126/science.1164857, 2009.

He, C., Li, Q. B., Liou, K. N., Zhang, J., Qi, L., Mao, Y., Gao, M., Lu, Z., Streets, D. G., Zhang, Q., Sarin, M. M., and Ram, K.: A global 3-D CTM evaluation of black carbon in the Tibetan Plateau, Atmospheric Chemistry and Physics, 14, 7091-7112, doi:10.5194/acp-14-7091-2014, 2014.

Herich, H., Hueglin, C., and Buchmann, B.: A 2.5 year's source apportionment study of black carbon from wood burning and fossil fuel combustion at urban and rural sites in Switzerland, Atmospheric Measurement Techniques, 4, 1409-1420, doi:10.5194/amt-4-1409-2011, 2011.

IPCC: Climate Change 2014: Synthesis Report. Contribution of Working Groups I, II and III to the Fifth Assessment Report of the Intergovernmental Panel on Climate Change, edited by: Core Writing Team, Pachauri, R. K. and Meyer, L. A., IPCC, Geneva, Switzerland, 151 pp, 2014.

Jacobson, M. Z.: Short-term effects of controlling fossil-fuel soot, biofuel soot and gases, and methane on climate, Arctic ice, and air pollution health, Journal of Geophysical Research, 115, D14209, doi:10.1029/2009jd013795, 2010.

Jenk, T., Szidat, S., Schwikowski, M., Gäggeler, H., Brütsch, S., Wacker, L., Synal, H.-A., and Saurer, M.: Radiocarbon analysis in an Alpine ice core: record of anthropogenic and biogenic contributions to carbonaceous aerosols in the past (1650–1940), Atmospheric chemistry and physics, 6, 5381-5390, doi: 10.5194/acp-6-5381-2006, 2006.

Kodros, J., and Pierce, J.: Important global and regional differences in aerosol cloud‐albedo effect estimates between simulations with and without prognostic aerosol microphysics, Journal of Geophysical Research: Atmospheres, 122, 4003-4018, doi: 10.1002/2016JD025886, 2017.

Konovalov, I. B., Lvova, D. A., Beekmann, M., Jethva, H., Mikhailov, E. F., Paris, J.-D., Belan, B. D., Kozlov, V. S., Ciais, P., and Andreae, M. O.: Estimation of black carbon emissions from Siberian fires using satellite observations of absorption and extinction optical depths, Atmos. Chem. Phys., 18, 14889-14924, https://doi.org/10.5194/acp-18-14889-2018, 2018.

Lee, Y., Chen, K., and Adams, P.: Development of a global model of mineral dust aerosol microphysics, Atmospheric Chemistry and Physics, 9, 2441-2458, doi: 10.5194/acp-9-2441-2009, 2009.

Li, C., Bosch, C., Kang, S., Andersson, A., Chen, P., Zhang, Q., Cong, Z., Chen, B., Qin, D., and Gustafsson, O.: Sources of black carbon to the Himalayan-Tibetan Plateau glaciers, Nat Commun, 7, 12574, doi: 10.1038/ncomms12574, 2016.

Li, M., Zhang, Q., Kurokawa, J.-i., Woo, J.-H., He, K., Lu, Z., Ohara, T., Song, Y., Streets, D. G., Carmichael, G. R., Cheng, Y., Hong, C., Huo, H., Jiang, X., Kang, S., Liu, F., Su, H., and Zheng, B.: MIX: a mosaic Asian anthropogenic emission inventory under the international collaboration framework of the MICS-Asia and HTAP, Atmospheric Chemistry and Physics, 17, 935-963, doi:10.5194/acp-17-935-2017, 2017.

Liu, H., Jacob, D. J., Bey, I., and Yantosca, R. M.: Constraints from 210Pb and 7Be on wet deposition and transport in a global three‐dimensional chemical tracer model driven by assimilated meteorological fields, Journal of Geophysical Research: Atmospheres, 106, 12109-12128, doi: 0148-0227/01/2000 JD900839, 2001.

Ma, P.-L., Rasch, P. J., Fast, J. D., Easter, R. C., Gustafson Jr, W., Liu, X., Ghan, S. J., and Singh, B.: Assessing the CAM5 physics suite in the WRF-Chem model: Implementation, resolution sensitivity, and a first evaluation for a regional case study, Geoscientific Model Development Discussion, 7, 755, doi:10.5194/gmd-7-755-2014, 2014.

McMeeking, G. R., Morgan, W. T., Flynn, M., Highwood, E. J., Turnbull, K., Haywood, J., and Coe, H.: Black carbon aerosol mixing state, organic aerosols and aerosol optical properties over the United Kingdom, Atmospheric Chemistry and Physics, 11, 9037-9052, doi:10.5194/acp-11-9037-2011, 2011.

Moteki, N., Kondo, Y., Miyazaki, Y., Takegawa, N., Komazaki, Y., Kurata, G., Shirai, T., Blake, D. R., Miyakawa, T., and Koike, M.: Evolution of mixing state of black carbon particles: Aircraft measurements over the western Pacific in March 2004, Geophysical Research Letters, 34, L11803, doi:10.1029/2006gl028943, 2007.

Mouteva, G. O., Randerson, J. T., Fahrni, S. M., Bush, S. E., Ehleringer, J. R., Xu, X., Santos, G. M., Kuprov, R., Schichtel, B. A., and Czimczik, C. I.: Using radiocarbon to constrain black and organic carbon aerosol sources in Salt Lake City, Journal of Geophysical Research: Atmospheres, 122, 9843-9857, doi:10.1002/2017jd026519, 2017.

Park, R. J., Jacob, D. J., Chin, M., and Martin, R. V.: Sources of carbonaceous aerosols over the United States and implications for natural visibility, Journal of Geophysical Research: Atmospheres, 108, 4355, doi: 10.1029/2002jd003190, 2003.

Park, R. J., Jacob, D. J., Palmer, P. I., Clarke, A. D., Weber, R. J., Zondlo, M. A., Eisele, F. L., Bandy, A. R., Thornton, D. C., and Sachse, G. W.: Export efficiency of black carbon aerosol in continental outflow: Global implications, Journal of Geophysical Research: Atmospheres, 110, D11205, doi: 10.1029/2004jd005432, 2005.

Petters, M., and Kreidenweis, S.: A single parameter representation of hygroscopic growth and cloud condensation nucleus activity, Atmospheric Chemistry and Physics, 7, 1961-1971, doi: 10.5194/acp-7-1961-2007, 2007.

Pierce, J., Chen, K., and Adams, P.: Contribution of primary carbonaceous aerosol to cloud condensation nuclei: processes and uncertainties evaluated with a global aerosol microphysics model, Atmospheric Chemistry and Physics, 7, 5447-5466, doi: 10.5194/acp-7-5447-2007, 2007.

Qi, L., Li, Q., He, C., Wang, X., and Huang, J.: Effects of the Wegener–Bergeron–Findeisen process on global black carbon distribution, Atmospheric Chemistry and Physics, 17, 7459-7479, doi:10.5194/acp-17-7459-2017, 2017a.

Qi, L., Li, Q., Henze, D. K., Tseng, H.-L., and He, C.: Sources of springtime surface black carbon in the Arctic: an adjoint analysis for April 2008, Atmospheric Chemistry and Physics, 17, 9697-9716, doi:10.5194/acp-17-9697-2017, 2017b.

Qi, L., Li, Q., Li, Y., and He, C.: Factors controlling black carbon distribution in the Arctic, Atmospheric Chemistry and Physics, 17, 1037-1059, doi:10.5194/acp-17-1037-2017, 2017c.

Reddy, C. M., Pearson, A., Xu, L., McNichol, A. P., Benner, B. A., Wise, S. A., Klouda, G. A., Currie, L. A., and Eglinton, T. I.: Radiocarbon as a tool to apportion the sources of polycyclic aromatic hydrocarbons and black carbon in environmental samples, Environmental Science & Technology, 36, 1774-1782, doi: 10.1021/es011343f , 2002.

Sahu, L. K., Kondo, Y., Moteki, N., Takegawa, N., Zhao, Y., Cubison, M. J., Jimenez, J. L., Vay, S., Diskin, G. S., Wisthaler, A., Mikoviny, T., Huey, L. G., Weinheimer, A. J., and Knapp, D. J.: Emission characteristics of black carbon in anthropogenic and biomass burning plumes over California during ARCTAS-CARB 2008, Journal of Geophysical Research: Atmospheres, 117, D16302, doi:10.1029/2011jd017401, 2012.

Samset, B. H., Myhre, G., Schulz, M., Balkanski, Y., Bauer, S., Berntsen, T. K., Bian, H., Bellouin, N., Diehl, T., Easter, R. C., Ghan, S. J., Iversen, T., Kinne, S., Kirkevåg, A., Lamarque, J. F., Lin, G., Liu, X., Penner, J. E., Seland, Ø., Skeie, R. B., Stier, P., Takemura, T., Tsigaridis, K., and Zhang, K.: Black carbon vertical profiles strongly affect its radiative forcing uncertainty, Atmospheric Chemistry and Physics, 13, 2423-2434, doi:10.5194/acp-13-2423-2013, 2013.

Samset, B. H., Myhre, G., Herber, A., Kondo, Y., Li, S. M., Moteki, N., Koike, M., Oshima, N., Schwarz, J. P., Balkanski, Y., Bauer, S. E., Bellouin, N., Berntsen, T. K., Bian, H., Chin, M., Diehl, T., Easter, R. C., Ghan, S. J., Iversen, T., Kirkevåg, A., Lamarque, J. F., Lin, G., Liu, X., Penner, J. E., Schulz, M., Seland, Ø., Skeie, R. B., Stier, P., Takemura, T., Tsigaridis, K., and Zhang, K.: Modelled black carbon radiative forcing and atmospheric lifetime in AeroCom Phase II constrained by aircraft observations, Atmospheric Chemistry and Physics, 14, 12465-12477, doi:10.5194/acp-14-12465-2014, 2014.

Sato, Y., Miura, H., Yashiro, H., Goto, D., Takemura, T., Tomita, H., and Nakajima, T.: Unrealistically pristine air in the Arctic produced by current global scale models, Scientific reports, 6, 26561, doi:10.1038/srep26561, 2016.

Schwarz, J. P., Gao, R. S., Spackman, J. R., Watts, L. A., Thomson, D. S., Fahey, D. W., Ryerson, T. B., Peischl, J., Holloway, J. S., Trainer, M., Frost, G. J., Baynard, T., Lack, D. A., de Gouw, J. A., Warneke, C., and Del Negro, L. A.: Measurement of the mixing state, mass, and optical size of individual black carbon particles in urban and biomass burning emissions, Geophysical Research Letters, 35, L13810, doi:10.1029/2008gl033968, 2008.

Shiraiwa, M., Kondo, Y., Moteki, N., Takegawa, N., Miyazaki, Y., and Blake, D. R.: Evolution of mixing state of black carbon in polluted air from Tokyo, Geophysical Research Letters, 34, L16803, doi:10.1029/2007gl029819, 2007.

Subramanian, R., Kok, G., Baumgardner, D., Clarke, A., Shinozuka, Y., Campos, T., Heizer, C., Stephens, B., De Foy, B., and Voss, P. B.: Black carbon over Mexico: the effect of atmospheric transport on mixing state, mass absorption cross-section, and BC/CO ratios, Atmospheric Chemistry & Physics, 10, 219-237, doi:10.5194/acp-10-219-2010, 2010.

Szidat, S., Jenk, T. M., Synal, H.-A., Kalberer, M., Wacker, L., Hajdas, I., Kasper-Giebl, A., and Baltensperger, U.: Contributions of fossil fuel, biomass-burning, and biogenic emissions to carbonaceous aerosols in Zurich as traced by14C, Journal of Geophysical Research, 111, doi:10.1029/2005jd006590, 2006.

Szidat, S., Ruff, M., Perron, N., Wacker, L., Synal, H.-A., Hallquist, M., Shannigrahi, A. S., Yttri, K. E., Dye, C., and Simpson, D.: Fossil and non-fossil sources of organic carbon (OC) and elemental carbon (EC) in Göteborg, Sweden, Atmospheric Chemistry and Physics, 9, 1521-1535, doi: 10.5194/acp-9-1521-2009, 2009.

van der Werf, G. R., Randerson, J. T., Giglio, L., Collatz, G. J., Mu, M., Kasibhatla, P. S., Morton, D. C., DeFries, R. S., Jin, Y., and van Leeuwen, T. T.: Global fire emissions and the contribution of deforestation, savanna, forest, agricultural, and peat fires (1997–2009), Atmospheric Chemistry and Physics, 10, 11707-11735, doi:10.5194/acp-10-11707-2010, 2010.

Wang, Q., Jacob, D. J., Fisher, J. A., Mao, J., Leibensperger, E. M., Carouge, C. C., Le Sager, P., Kondo, Y., Jimenez, J. L., Cubison, M. J., and Doherty, S. J.: Sources of carbonaceous aerosols and deposited black carbon in the Arctic in winter-spring: implications for radiative forcing, Atmospheric Chemistry and Physics, 11, 12453-12473, doi:10.5194/acp-11-12453-2011, 2011.

Winiger, P., Andersson, A., Yttri, K. E., Tunved, P., and Gustafsson, O.: Isotope-Based Source Apportionment of EC Aerosol Particles during Winter High-Pollution Events at the Zeppelin Observatory, Svalbard, Environ Sci Technol, 49, 11959-11966, doi:10.1021/acs.est.5b02644, 2015.

Winiger, P., Andersson, A., Eckhardt, S., Stohl, A., and Gustafsson, Ö.: The sources of atmospheric black carbon at a European gateway to the Arctic, Nature Communications, 7, 12776, doi:10.1038/ncomms12776, 2016.

Winiger, P., Andersson, A., Eckhardt, S., Stohl, A., Semiletov, I. P., Dudarev, O. V., Charkin, A., Shakhova, N., Klimont, Z., Heyes, C., and Gustafsson, O.: Siberian Arctic black carbon sources constrained by model and observation, Proc Natl Acad Sci U S A, 114, E1054-E1061, doi:10.1073/pnas.1613401114, 2017.

Winiger, P., Barrett, T. E., Sheesley, R. J., Huang, L., Sharma, S., Barrie, L. A., Yttri, K. E., Evangeliou, N., Eckhardt, S., Stohl, A., Klimont, Z., Heyes, C., Semiletov, I. P., Dudarev, O. V., Charkin, A., Shakhova, N., Holmstrand, H., Andersson, A., and Gustafsson, Ö.: Source apportionment of circum-Arctic atmospheric black carbon from isotopes and modeling, Science Advances, 5, eaau8052, doi:10.1126/sciadv.aau8052, 2019.

Yamamoto, N., Muramoto, A., Yoshinaga, J., Shibata, K., Endo, M., Endo, O., Hirabayashi, M., Tanabe, K., Goto, S., and Yoneda, M.: Comparison of carbonaceous aerosols in Tokyo before and after implementation of diesel exhaust restrictions, Environmental science & technology, 41, 6357-6362, doi:10.1021/acs.est.5b02644, 2007.

Zhang, Y. L., Perron, N., Ciobanu, V. G., Zotter, P., Minguillón, M. C., Wacker, L., Prévôt, A. S. H., Baltensperger, U., and Szidat, S.: On the isolation of OC and EC and the optimal strategy of radiocarbon-based source apportionment of carbonaceous aerosols, Atmospheric Chemistry and Physics, 12, 10841-10856, doi:10.5194/acp-12-10841-2012, 2012.

Zhang, Y. L., Huang, R. J., El Haddad, I., Ho, K. F., Cao, J. J., Han, Y., Zotter, P., Bozzetti, C., Daellenbach, K. R., Canonaco, F., Slowik, J. G., Salazar, G., Schwikowski, M., Schnelle-Kreis, J., Abbaszade, G., Zimmermann, R., Baltensperger, U., Prévôt, A. S. H., and Szidat, S.: Fossil vs. non-fossil sources of fine carbonaceous aerosols in four

Chinese cities during the extreme winter haze episode of 2013, Atmospheric Chemistry and Physics, 15, 1299-1312, doi:10.5194/acp-15-1299-2015, 2015.

Zotter, P., Ciobanu, V. G., Zhang, Y. L., El-Haddad, I., Macchia, M., Daellenbach, K. R., Salazar, G. A., Huang, R.-J., Wacker, L., Hueglin, C., Piazzalunga, A., Fermo, P., Schwikowski, M., Baltensperger, U., Szidat, S., and Prévôt, A. S. H.: Radiocarbon analysis of elemental and organic carbon in Switzerland during winter-smog episodes from 2008 to 2012 – Part 1: Source apportionment and spatial variability, Atmospheric Chemistry and Physics, 14, 13551- 13570, https://doi.org/10.5194/acp-14-13551-2014, 2014.

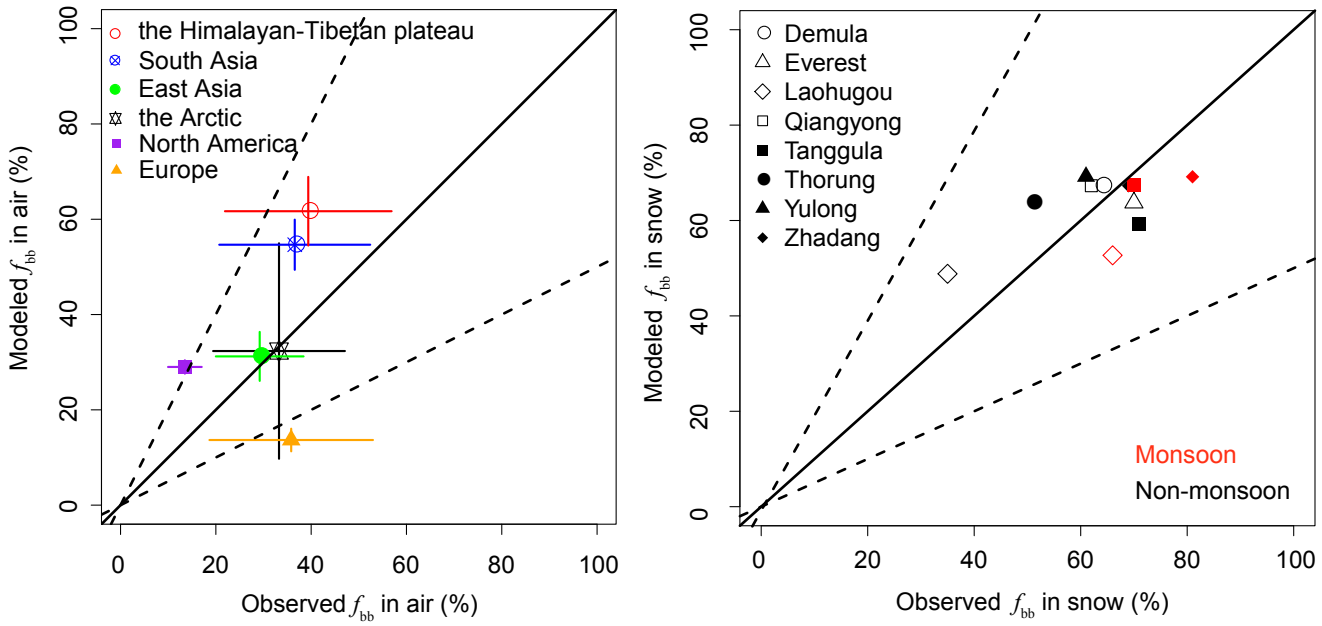

Figure 1: Observed and GEOS-Chem simulated fraction of biomass burning (f_{bb}, %) of (a) BC in the atmosphere in the Arctic, South Asia, North America, Europe, East Asia, and the Himalayan-Tibetan plateau (the regions are symbol and color coded, see data in Table S2.) and (b) BC in snow during monsoon (red) and non-monsoon (black) seasons over the Himalayan-Tibetan plateau. Also shown in (a) are the standard deviations of observed and model simulated f_{bb} in each region, reflecting the temporal and spatial variations of f_{bb} in the region (horizontal and vertical lines). Observations of f_{bb} in the atmosphere in (a) are from carbon isotope analysis as listed in Table S1. Observations of f_{bb} in BC in snow in (b) are from Li et al. (2016). Solid lines in (a) and (b) are 1:1 ratio lines and dashed lines are 1:2 (or 2:1).

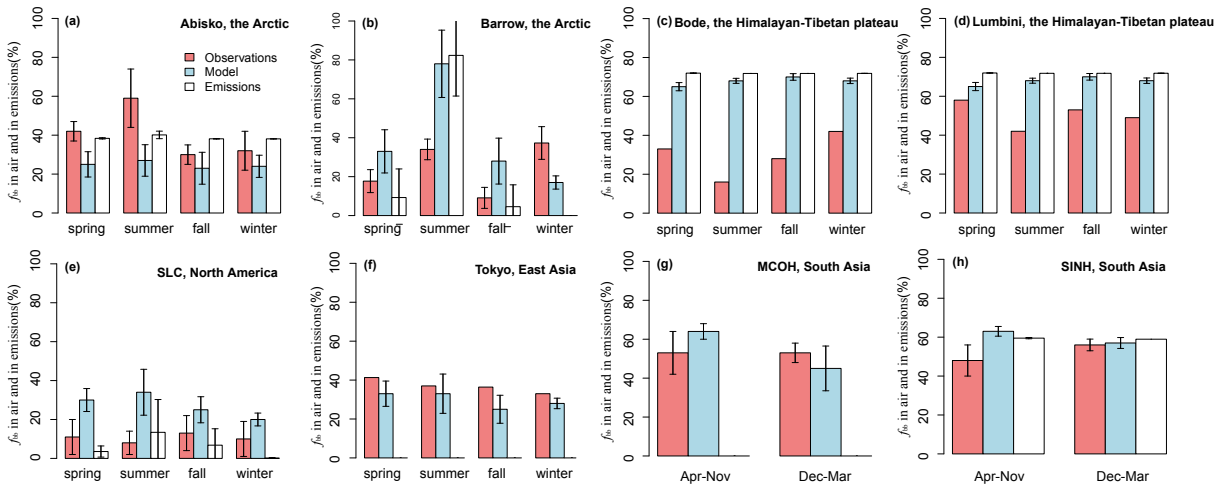

Figure 2: Seasonal variations of observed (lightcoral bars) and GEOS-Chem simulated (lightblue bars) f_{bb} of BC in the atmosphere at (a) Abisko and (b) Barrow in the Arctic, (c) Bode and (d) Lumbini over the Himalayan–Tibetan Plateau, (e) Salt Lake City in North America, (f) Tokyo in East Asia, (g) MCOH and (h) SINH in South Asia. The white bars are f_{bb} values of BC emissions in the model grid (4° lat x 5° lon) of each site. Also shown are the standard deviations (error bars). Site locations are shown in Fig. S3.

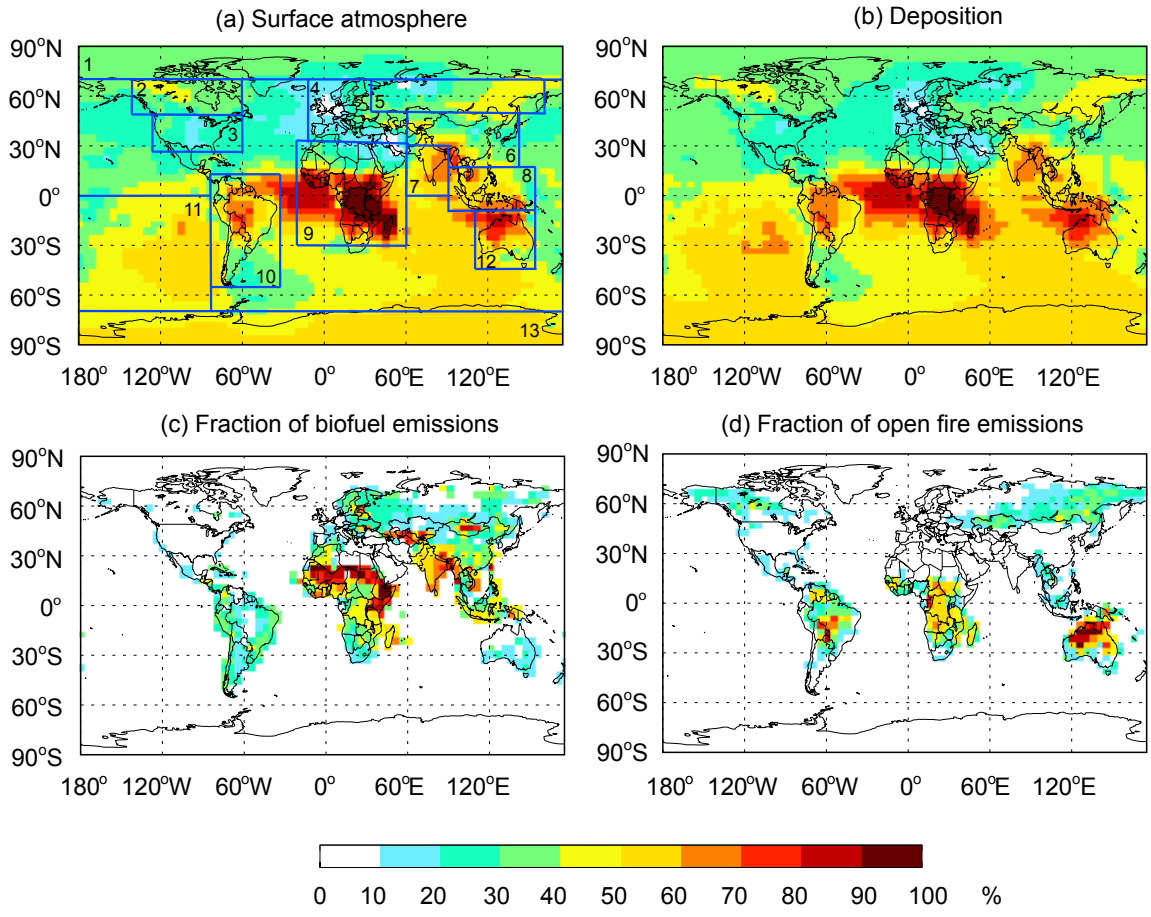

Figure 3: Annual (a) f_{bb} of BC in the atmosphere at surface, (b) f_{bb} of BC deposition, (c) fraction of biofuel emissions and (d) fraction of open fire emissions. Data are averaged for 2007–2013. Also shown in (a) are regions discussed in the text: 1. the Arctic, 2. Canada, 3. the US, 4. Europe, 5. Siberia, 6. East (E.) Asia, 7. South (S.) Asia, 8. Southeast (SE.) Asia, 9. Africa, 10. S. America, 11. S. Pacific, 12. Australia, and 13. the Antarctic.

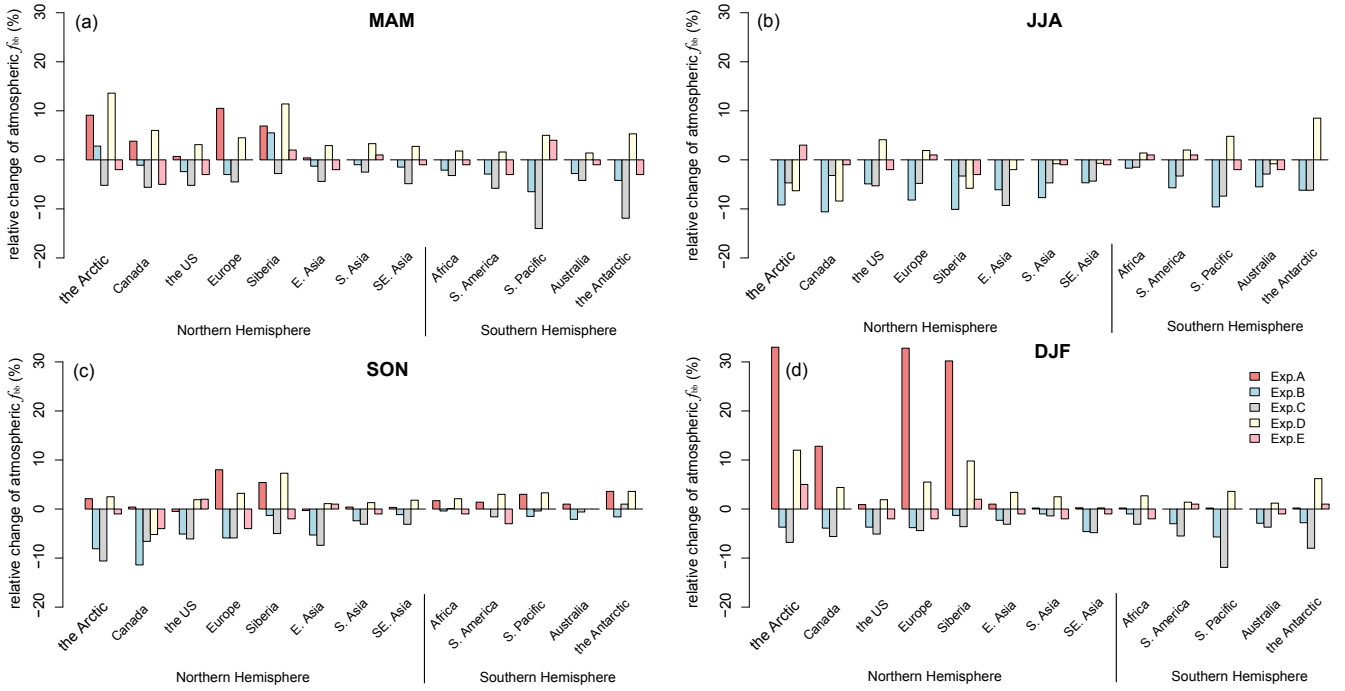

Figure 4: GEOS-Chem simulated fractional change (r) to atmospheric f_{bb} relative to the standard simulation, as a result of doubled biofuel emissions north of 45°N (Exp. A), 70% of hydrophilic BC in freshly emitted biomass burning BC-containing particles (Exp. B), 4 hour e-folding aging time of BC in biomass burning plumes and linear aging rate of 1% in fossil fuel plumes (Exp. C), TOMAS microphysical aging and scavenging (Exp. D) and finer horizontal model resolution (2° lat × 2.5° lon, Exp. E), $r = ([f_{bb}]_{Exp.} - [f_{bb}]_{Std.})/[f_{bb}]_{Std.}$, that varies with regions (see region definition in Fig.3 (a)) and seasons ((a) March–May (MAM), (b) June–August (JJA), (c) September–November (SON) and (d) December–February (DJF)), averaged for 2007–2013. See details of the standard simulation and the uncertainty experiments in the text.

Table S1. Carbon isotope analysis of BC sources (fossil fuel versus biomass burning) in the atmosphere

Pt	Region	Site	Lat	Lon	Alt (m)	Year	Mon	Season	f_{bb} (%)	BC isolation method	References
1	Arctic	Zeppelin	78.9	11.9	478	2009	Jan-Mar	winter	52±15[5]	NIOSH 5040[6]	Winiger et al., 2015
2	Arctic	Abisko	68.4	19.1	359	2011-13	Jan-Mar	winter	35±10	NIOSH 5040	Winiger et al., 2016
3	Arctic	Abisko	68.4	19.1	359	2011-13	Apr-Aug	summer	58±15	NIOSH 5040	Winiger et al., 2016
4	Arctic	Barrow	71.2	-156.6	11	2012-13	Dec-Feb	winter	32±9	NIOSH 5040	Barrett et al., 2015
5	Arctic	Barrow	71.2	-156.6	11	2012-13	Feb Mar	winter	51±6	NIOSH 5040	Barrett et al., 2015
6	Arctic	Barrow	71.2	-156.6	11	2013	Mar-May	spring	18±7	NIOSH 5040	Winiger et al., 2019
7	Arctic	Barrow	71.2	-156.6	11	2013	Jul-Aug	summer	34±5	NIOSH 5040	Winiger et al., 2019
8	Arctic	Barrow	71.2	-156.6	11	2013	Sep-Nov	fall	9±5	NIOSH 5040	Winiger et al., 2019
9	Arctic	Barrow	71.2	-156.6	11	2013	Dec-Feb	winter	34±9	NIOSH 5040	Winiger et al., 2019
10	Arctic	Alert	82.3	-62.3	210	2014-15	Feb	winter	39±5	NIOSH 5040	Winiger et al., 2019
12	Arctic	Alert	82.3	-62.3	210	2014-15	Mar	spring	39±5	NIOSH 5040	Winiger et al., 2019
13	Arctic	Alert	82.3	-62.3	210	2014	May	spring	39±5	NIOSH 5040	Winiger et al., 2019
11	Arctic	Alert	82.3	-62.3	210	2014	Jul	summer	37±5	NIOSH 5040	Winiger et al., 2019
14	Arctic	Alert	82.3	-62.3	210	2014	Nov	fall	40±5	NIOSH 5040	Winiger et al., 2019
15	Arctic	Alert	82.3	-62.3	210	2014	Dec	winter	44±5	NIOSH 5040	Winiger et al., 2019
16	Arctic	Tiksi	71.4	128.5	11	2012-14	Mar-May	spring	25±0.2	NIOSH 5040	Winiger et al., 2017
17	Arctic	Tiksi	71.4	128.5	11	2012-14	Jun-Aug	summer	45±0.1	NIOSH 5040	Winiger et al., 2017
18	Arctic	Tiksi	71.4	128.5	11	2012-14	Sep-Nov	fall	48±0.1	NIOSH 5040	Winiger et al., 2017
19	Arctic	Tiksi	71.4	128.5	11	2012-14	Dec-Feb	winter	28±0.2	NIOSH 5040	Winiger et al., 2017
20	South Asia	MCOH[1]	6.8	73.3	15	2006	Jan_Mar	winter	68±6	NIOSH 5040	Gustafsson et al., 2009
21	South Asia	MCOH	6.8	73.3	15	2008-09	Dec_Mar	winter	53±5	NIOSH 5040	Budhavant et al., 2015
22	South Asia	MCOH	6.8	73.3	15	2008-09	Mar_Nov	summer	53±11	NIOSH 5040	Budhavant et al., 2015
23	South Asia	SINH[2]	18.3	73.7	1450	2006	Mar_Apr	spring	46±8	NIOSH 5040	Gustafsson et al., 2009
24	South Asia	SINH	18.3	73.7	1450	2008-09	Dec_Mar	winter	56±3	NIOSH 5040	Budhavant et al., 2015
25	South Asia	SINH	18.3	73.7	1450	2008-09	Mar_Nov	summer	48±8	NIOSH 5040	Budhavant et al., 2015
26	South Asia	Delhi	28.5	77.2	300	2011	Dec-Feb	witner	39	NIOSH 5040	Bikkina et al., 2019
27	South Asia	Delhi	28.5	77.2	300	2011	Mar-May	spring	24	NIOSH 5040	Bikkina et al., 2019
28	South Asia	Delhi	28.5	77.2	300	2011	Jun-Aug	summer	17	NIOSH 5040	Bikkina et al., 2019
29	South Asia	Delhi	28.5	77.2	300	2011	Sep-Nov	fall	31	NIOSH 5040	Bikkina et al., 2019
30	Europe	Göteborg	57.7	11.9	20	2005	Feb	winter	12±4	THEODORE[7]	Szidat et al., 2009
31	Europe	Göteborg	57.7	11.9	20	2006	Jun	summer	12±3	THEODORE	Szidat et al., 2009
32	Europe	Råö	57.3	11.9	10	2005	Feb	winter	38±5	THEODORE	Szidat et al., 2009
33	Europe	Zurich	47.3	8.5	410	2002	Aug	summer	8±1	THEODORE	Szidat et al., 2004
34	Europe	Zurich	47.3	8.5	410	2003	Feb	winter	29±5	THEODORE	Szidat et al., 2006

35	Europe	Zurich	47.3	8.5	410	2003	Mar	spring	15±5	THEODORE	Szidat et al., 2006
36	Europe	Zurich	47.3	8.5	410	2006	Jan	winter	29±4	THEODORE	Sandradewi et al., 2008a
37	Europe	Dübendorf	47.4	8.6	440	2007	Oct	fall	36±3	Swiss_4S[8]	Zhang et al., 2012
38	Europe	Roveredo	46.2	9.1	298	2005	Jan	winter	60±6	THEODORE	Szidat et al., 2007
39	Europe	Roveredo	46.2	9.1	298	2005	Mar	spring	58±6	THEODORE	Szidat et al., 2007
40	Europe	Roveredo	46.2	9.1	298	2005	Dec	winter	74±10	THEODORE	Sandradewi et al., 2008b
41	Europe	Roveredo	46.2	9.1	370	07/08-	Dec-Feb	winter	46	Swiss_4S	Zotter et al., 2014
42	Europe	Moleno	46.3	8.9	254	2005	Feb	winter	17±7	THEODORE	Szidat et al., 2007
43	Europe	Moleno	46.3	8.99	305	07/08-	Dec-Feb	winter	28	Swiss_4S	Zotter et al., 2014
44	Europe	Reiden	47.2	7.9	457	2006	Feb	winter	30±4	THEODORE	Sandradewi et al., 2008a
45	Europe	Reiden	47.2	7.9	510	07/08-	Dec-Feb	winter	34	Swiss_4S	Zotter et al., 2014
46	Europe	Massongex	46.2	6.1	400	2006	Nov	fall	36±4	THEODORE	Perron et al., 2010
47	Europe	Massongex	46.2	6.1	400	2006	Dec	winter	36±4	THEODORE	Perron et al., 2010
48	Europe	Massongex	46.2	6.1	452	08/09-11/12	Dec-Feb	winter	54	Swiss_4S	Zotter et al., 2014
49	Europe	Saxon	46.1	7.1	460	2006	Dec	winter	32±4	THEODORE	Perron et al., 2010
50	Europe	Sion	46.2	7.3	505	2006	Dec	winter	20±3	THEODORE	Perron et al., 2010
51	Europe	Brigerbad	46.3	7.9	650	2006	Dec	winter	31±4	THEODORE	Perron et al., 2010
52	Europe	Payerne	46.8	6.9	456	2006	Jan	winter	60±4	Swiss_4S	Zhang et al., 2012
53	Europe	Payerne	46.8	6.9	456	2006	Jun	summer	44±3	Swiss_4S	Zhang et al., 2012
54	Europe	Payerne	46.8	6.9	539	07/08-11/12	Dec-Feb	winter	51	Swiss_4S	Zotter et al., 2014
55	Europe	Barcelona	41.3	2.1	80	2009	Mar	spring	15±3	adapted THEODORE	Minguillón et al., 2011
56	Europe	Barcelona	41.3	2.1	80	2009	Jul	summer	9±4	adapted THEODORE	Minguillón et al., 2011
57	Europe	Montseny	41.8	2.3	720	2009	Mar	spring	37±4	adapted THEODORE	Minguillón et al., 2011
58	Europe	Montseny	41.8	2.3	720	2009	Jul	summer	23±5	adapted THEODORE	Minguillón et al., 2011
59	Europe	Bern-Bollwerk	46.9	7.6	506	08/09-12/13	Dec-Feb	winter	22	Swiss_4S	Zotter et al., 2014
60	Europe	Sissach-West	47.5	7.8	410	07/08-11/12	Dec-Feb	winter	43	Swiss_4S	Zotter et al., 2014
61	Europe	St.Gallen-Rorschacherstrasse	47.4	9.4	457	07/08-11/12	Dec-Feb	winter	38	Swiss_4S	Zotter et al., 2014
62	Europe	Vaduz-Austrasse	47.1	9.5	706	07/08-11/12	Dec-Feb	winter	45	Swiss_4S	Zotter et al., 2014
63	Europe	Zôrich-Kaserne	47.3	8.5	457	07/08-	Dec-Feb	winter	41	Swiss_4S	Zotter et al., 2014

						11/12					
64	Europe	Basel-St.Johann	47.6	7.6	308	07/08-08/09	Dec-Feb	winter	41	Swiss_4S	Zotter et al., 2014
65	Europe	Solothurn-Altwyberhôsli	47.1	7.6	502	07/08-11/12	Dec-Feb	winter	46	Swiss_4S	Zotter et al., 2014
66	Europe	Sch_chental	46.8	8.8	995	10/11-	Dec-Feb	winter	67	Swiss_4S	Zotter et al., 2014
67	Europe	Chiasso	45.8	9	291	07/08-11/12	Dec-Feb	winter	41	Swiss_4S	Zotter et al., 2014
68	Europe	Magadino-Cadenazzo	46.8	6.9	254	07/08-11/12	Dec-Feb	winter	48	Swiss_4S	Zotter et al., 2014
69	Europe	San-Vittore	46.2	9.1	330	07/08-11/12	Dec-Feb	winter	66	Swiss_4S	Zotter et al., 2014
70	North America	Salt Lake City	40.7	-111.8	1426	2012-14	annual	summer	11±1.1	adapted Swiss_4S	Mouteva et al., 2017
71	North America	Mexico City	19.5	-99.1	2240	2006	Mar	spring	16±4	THEODORE	Aiken et al., 2010
72	East Asia	Tokyo	35.6	139.6	40	2004	Oct	fall	36.4	adapted IMPROVE[9]	Yamamoto et al., 2007
73	East Asia	Tokyo	35.6	139.6	40	2004	Dec	winter	33.8	adapted IMPROVE	Yamamoto et al., 2007
74	East Asia	Tokyo	35.6	139.6	40	2004	Feb	winter	32.6	adapted IMPROVE	Yamamoto et al., 2007
75	East Asia	Tokyo	35.6	139.6	40	2004	Apr	spring	41.3	adapted IMPROVE	Yamamoto et al., 2007
76	East Asia	Tokyo	35.6	139.6	40	2004	Jun	summer	37.7	adapted IMPROVE	Yamamoto et al., 2007
77	East Asia	Tokyo	35.6	139.6	40	2004	Aug	summer	35.8	adapted IMPROVE	Yamamoto et al., 2007
79	East Asia	Beijing	39.9	116.4	55	2013	Jan	winter	30±2	Swiss_4S	Zhang et al., 2015
80	East Asia	Beijing	39.9	116.4	55	2013	Jan	winter	26±2	NIOSH 5040	Andersson et al., 2015
81	East Asia	Beijing	39.9	116.4	55	2010	Feb	winter	17±4	NIOSH 5040	Chen et al., 2013
82	East Asia	Shanghai	31.3	121.5	4	2013	Jan	winter	21±2	Swiss_4S	Zhang et al., 2015
83	East Asia	Shanghai	31.3	121.5	4	2013	Jan	winter	32±2	NIOSH 5040	Andersson et al., 2015
84	East Asia	Shanghai	31.3	121.5	4	2010	Jan	winter	17±4	NIOSH 5040	Chen et al., 2013
85	East Asia	Guangzhou	23.1	113.4	15	2013	Jan	winter	48±5	Swiss_4S	Zhang et al., 2015
86	East Asia	Guangzhou	23.1	113.4	15	2013	Jan	winter	32±2	NIOSH 5040	Andersson et al., 2015
89	East Asia	Xi'an	34.2	108.9	416	2013	Jan	winter	25±3		Zhang et al., 2015
90	East Asia	Xiamen	24.5	118	2	2009	Dec	winter	13±3	NIOSH 5040	Chen et al., 2013
93	East Asia	KCOG[3]	33.3	126.2	72	2011	Mar	winter	25±6	NIOSH 5040	Chen et al., 2013
94	East Asia	SCCO[4]	24.6	118.1	3	2009	Jan	winter	22±3	NIOSH 5040	Chen et al., 2013
95	Tibet	Jilong	28.2	86	4166	2013	Apr	spring	45	NIOSH 5040	Li et al., 2016
96	Tibet	Jilong	28.2	86	4166	2013	Jun	winter	41	NIOSH 5040	Li et al., 2016
97	Tibet	Nielamu	28.2	86	4166	2013	Nov	fall	40	NIOSH 5040	Li et al., 2016
98	Tibet	Dhunche	28.1	85.3	2051	2014	Jan	winter	49	NIOSH 5040	Li et al., 2016
99	Tibet	Dhunche	28.1	85.3	2051	2013	Aug	summer	16	NIOSH 5040	Li et al., 2016

100	Tibet	Dhunche	28.1	85.3	2051	2013	Sep	fall	41	NIOSH 5040	Li et al., 2016
101	Tibet	Bode	27.7	85.4	1386	2014	Jan	winter	42	NIOSH 5040	Li et al., 2016
102	Tibet	Bode	27.7	85.4	1386	2013	Apr	spring	33	NIOSH 5040	Li et al., 2016
103	Tibet	Bode	27.7	85.4	1386	2013	Aug	summer	16	NIOSH 5040	Li et al., 2016
104	Tibet	Bode	27.7	85.4	1386	2013	Nov	fall	28	NIOSH 5040	Li et al., 2016
105	Tibet	Zhongba	29.7	84	4704	2013	Apr	spring	70	NIOSH 5040	Li et al., 2016
106	Tibet	Jomsom	28.8	83.7	3048	2013	Apr	spring	57	NIOSH 5040	Li et al., 2016
107	Tibet	Pokhara	28.2	84	813	2013	Jul	summer	26	NIOSH 5040	Li et al., 2016
108	Tibet	Pokhara	28.2	84	813	2013	Apr	spring	65	NIOSH 5040	Li et al., 2016
109	Tibet	Lumbini	27.5	83.3	100	2013	Apr	spring	58	NIOSH 5040	Li et al., 2016
110	Tibet	Lumbini	27.5	83.3	100	2013	Jul	summer	42	NIOSH 5040	Li et al., 2016
111	Tibet	Lumbini	27.5	83.3	100	2013	Oct	fall	53	NIOSH 5040	Li et al., 2016
112	Tibet	Lumbini	27.5	83.3	100	2013	Dec	winter	49	NIOSH 5040	Li et al., 2016
113	Tibet	Namco	30.8	91	4730	2013	Apr	spring	54	NIOSH 5040	Li et al., 2016
114	Tibet	Namco	30.8	91	4730	2014	Jun	summer	63	NIOSH 5040	Li et al., 2016
115	Tibet	Namco	30.8	91	4730	2014	Jul	summer	49	NIOSH 5040	Li et al., 2016
116	Tibet	Namco	30.8	91	4730	2013	Nov	fall	58	NIOSH 5040	Li et al., 2016
117	Tibet	Lulang	29.8	94.7	3326	2014	Jun	summer	20	NIOSH 5040	Li et al., 2016
118	Tibet	Lulang	29.8	94.7	3326	2014	Jul	summer	23	NIOSH 5040	Li et al., 2016
119	Tibet	Lhasa	29.6	91	3640	2014	Jan	winter	18	NIOSH 5040	Li et al., 2016
120	Tibet	Lhasa	29.6	91	3640	2013	Apr	spring	24	NIOSH 5040	Li et al., 2016
121	Tibet	Lhasa	29.6	91	3640	2013	Jun	summer	7	NIOSH 5040	Li et al., 2016

[1] Maldives Climate Observatory in Hanimaadhoo

[2] Indian Institute of Tropical Meteorology in Sinhagad, India

[3] Korea Climate Observatory-Gosan

[4] South China Climate Observatory

[5] Standard deviation of observations

[6] National Institute for Occupational Safety and Health 5040

[7] Two-step Heating system for the EC/OC Determination of Radiocarbon in the Environment

[8] four-step (S1, S2, S3 and S4) thermal-optical protocol

[9] Integragency Monitoring of Protected Visual Environments

Table S2 Observed and GEOS-Chem simulated atmospheric f_{bb} in various regions (%)

Region	Observations	Simulation
The Himalayan-Tibetan plateau	39±17*	62±7
South Asia	37±16	55±5
East Asia	29±9	31±5
The Arctic	33±14	32±23
North America	14±4	29±2
Europe	43±16	14±3

*Standard deviation, reflecting variations of atmospheric f_{bb} among different sites during different seasons in each region.

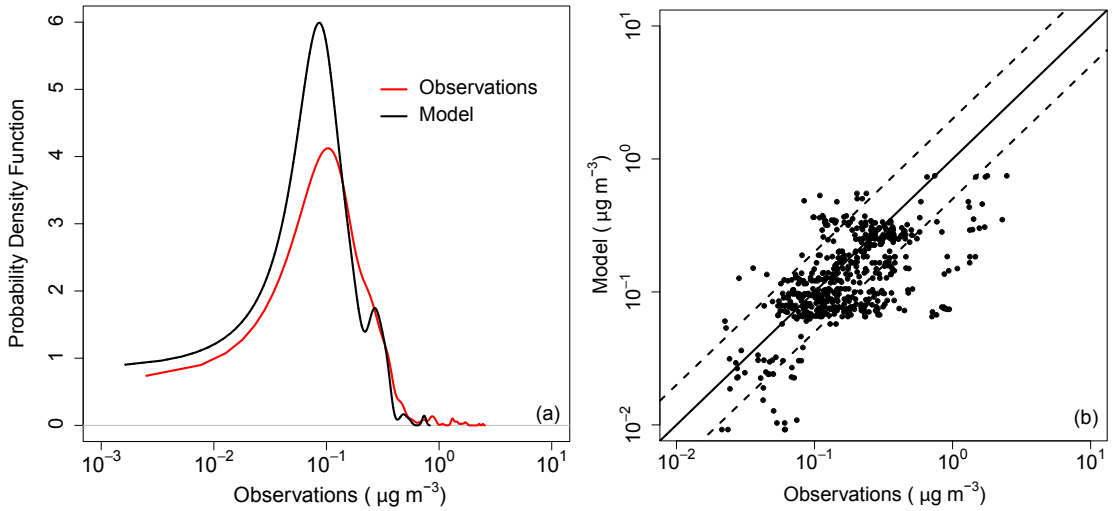

Figure S1. (a) Probability density function of observed (red line) and GEOS-Chem simulated (black) BC concentrations in surface air (µg m^{-3}) and (b) Observed and GEOS-Chem simulated annual BC concentrations in surface air. Data are for 2007–2013. Solid line is 1:1 ratio line and dashed lines are 1:2 (or 2:1).

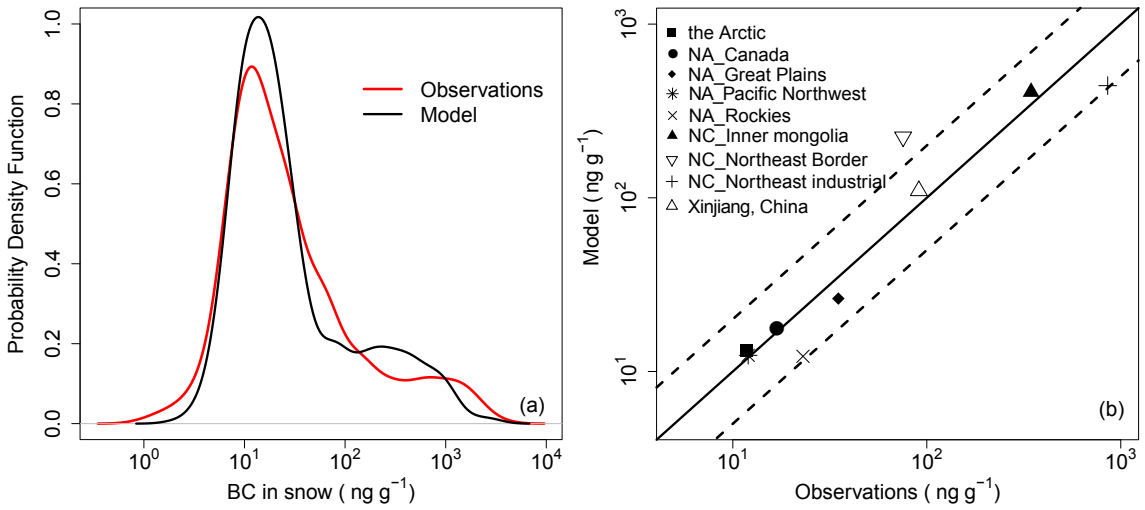

Figure S2. (a) Probability density function of observed (red line) and GEOS-Chem simulated (black) BC concentration in snow (ng g^{-1}) and (b) medians of observed and simulated BC in snow (ng g^{-1}) in the Arctic, North America (Canada, the Great Plains, the Pacific Northwest, and the Rockies, as defined in Doherty et al., 2014)), Northern China (Inner Mongolia, Northeast Border and Northeast Industrial, as defined by Wang et al., 2013), and Xinjiang, China. The regions are symbol-coded. Solid line – 1:1 ratio line; dashed lines – 1:2 (or 2:1) ratio lines.

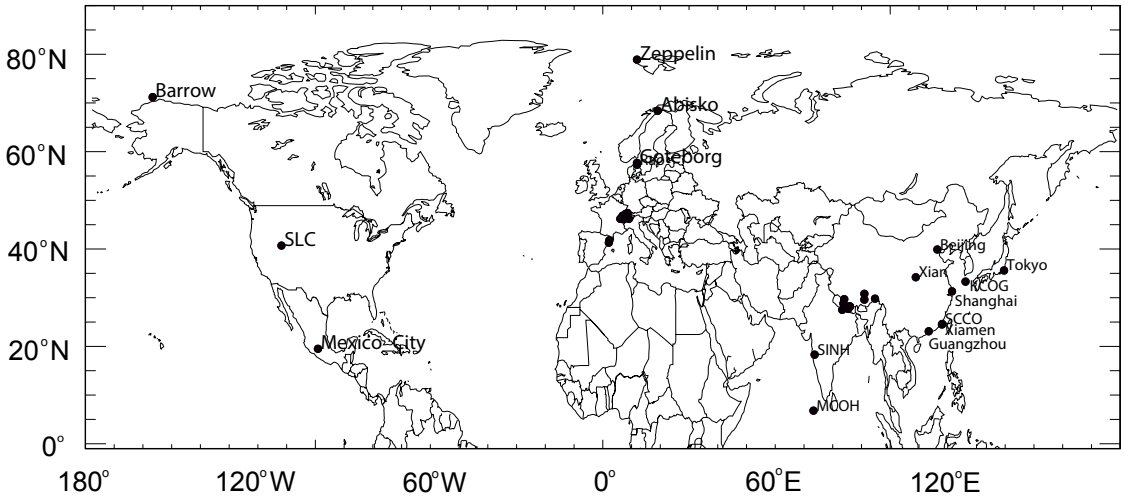

Figure S3. Carbon isotope measurement stations of BC as listed in Table S1.

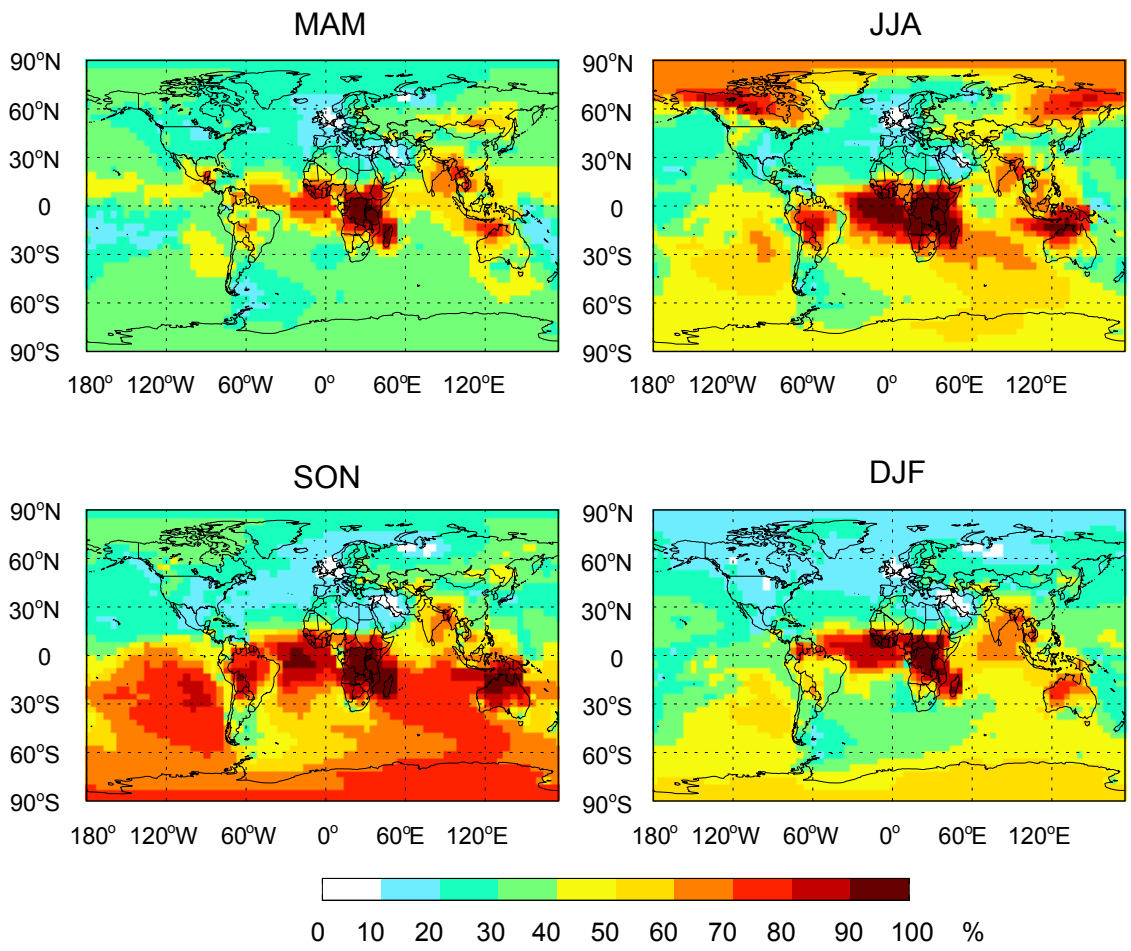

Figure S4. Average f_{bb} of BC in surface atmosphere during March–May (MAM), June–August (JJA), September–November (SON) and December–February (DJF) for 2007–2013.

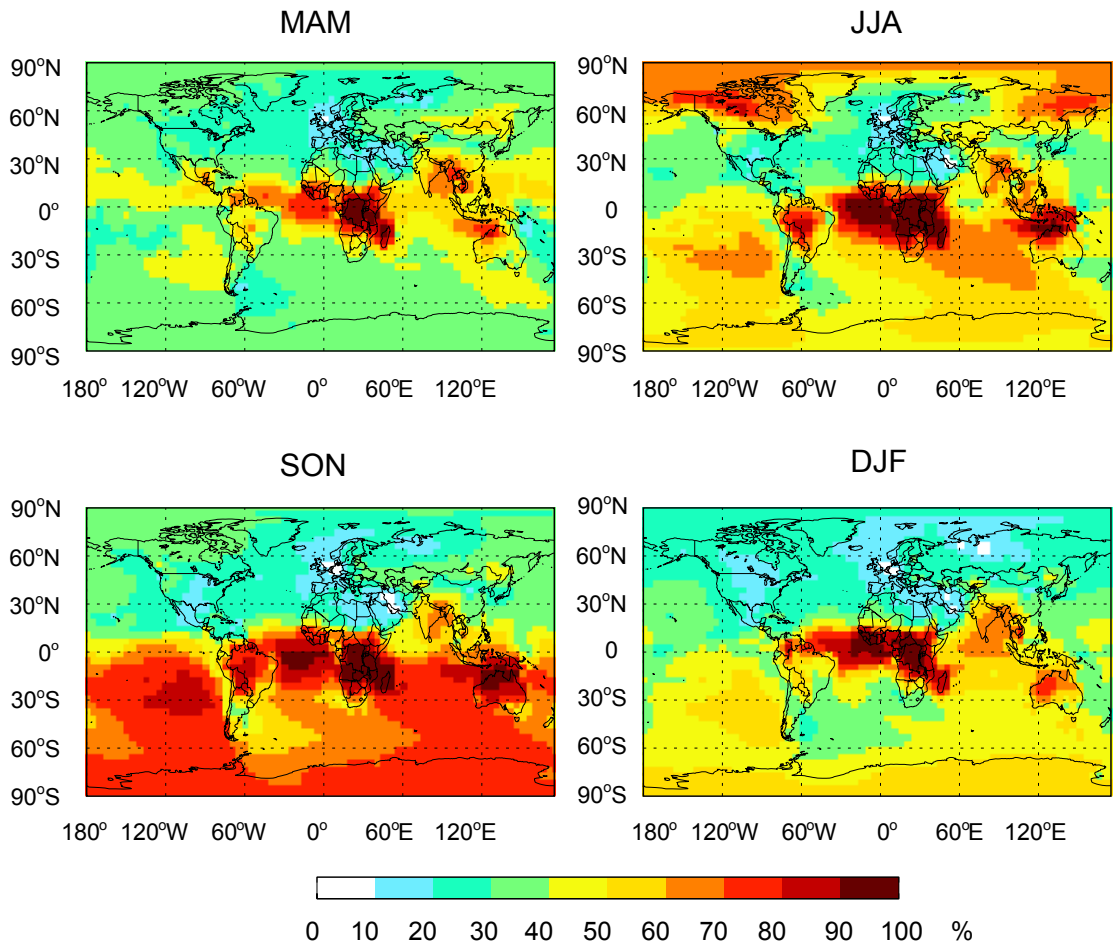

Figure S5. Same as Figure S4, but for BC deposition.

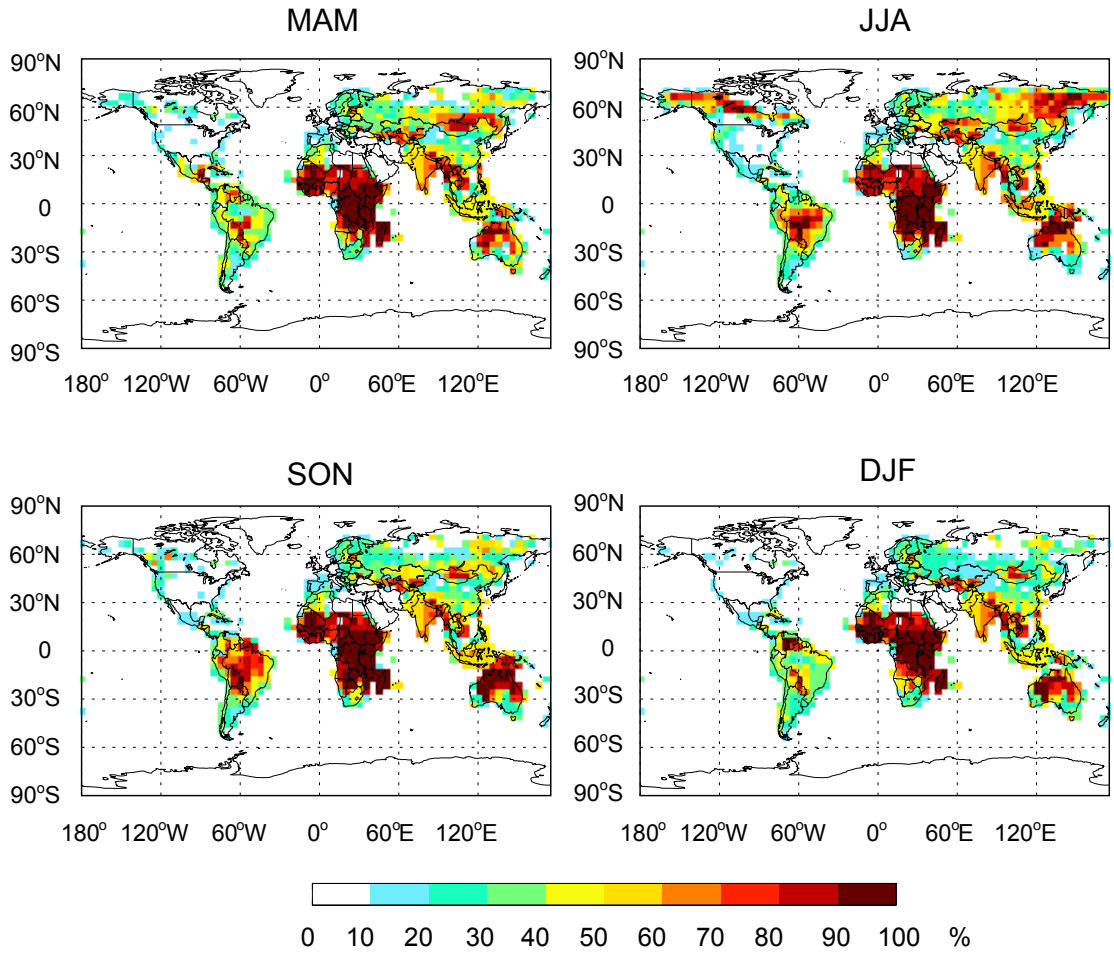

Figure S6. Same as Figure S4, but for BC emissions.

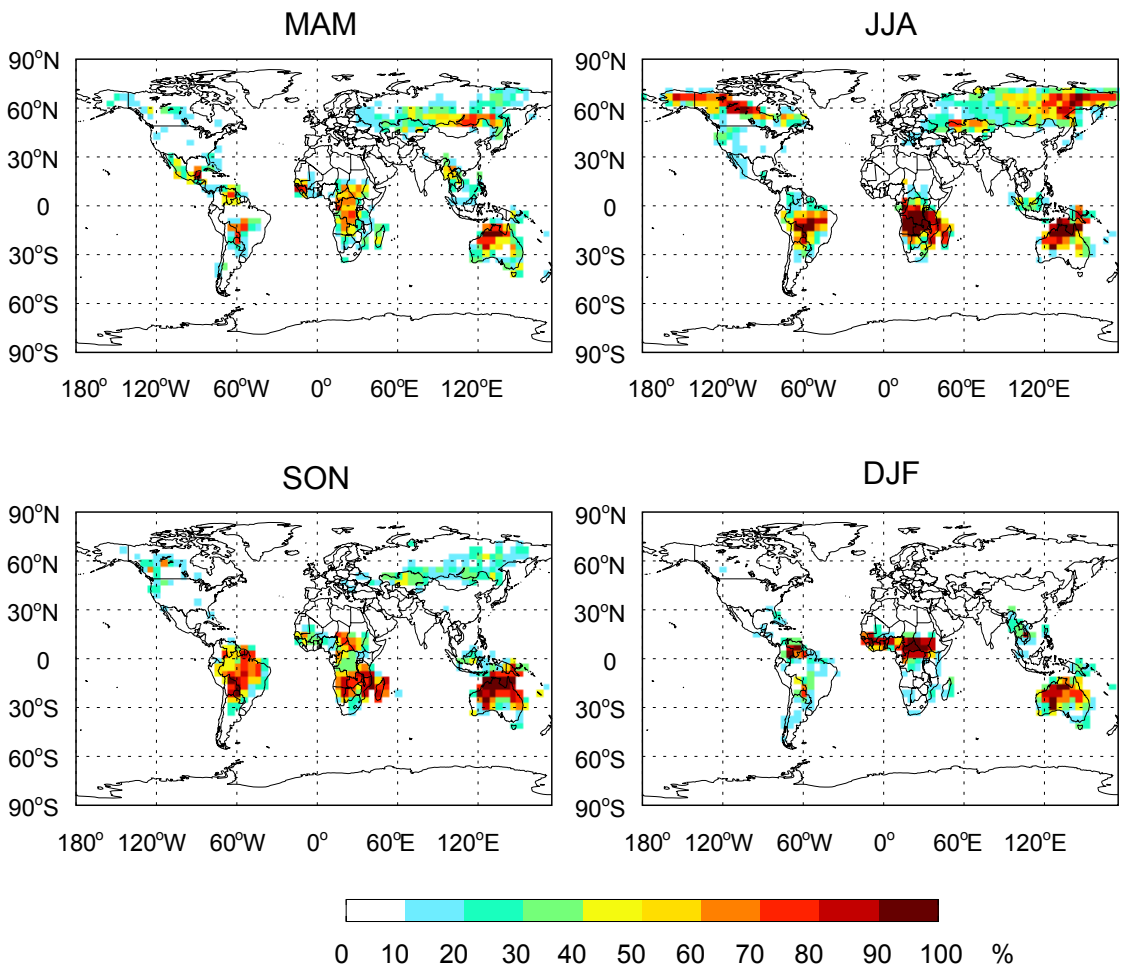

Figure S7. Average contribution of open burning to BC emissions (%) during March–May (MAM), June–August (JJA), September–November (SON) and December–February (DJF) for 2007–2013.

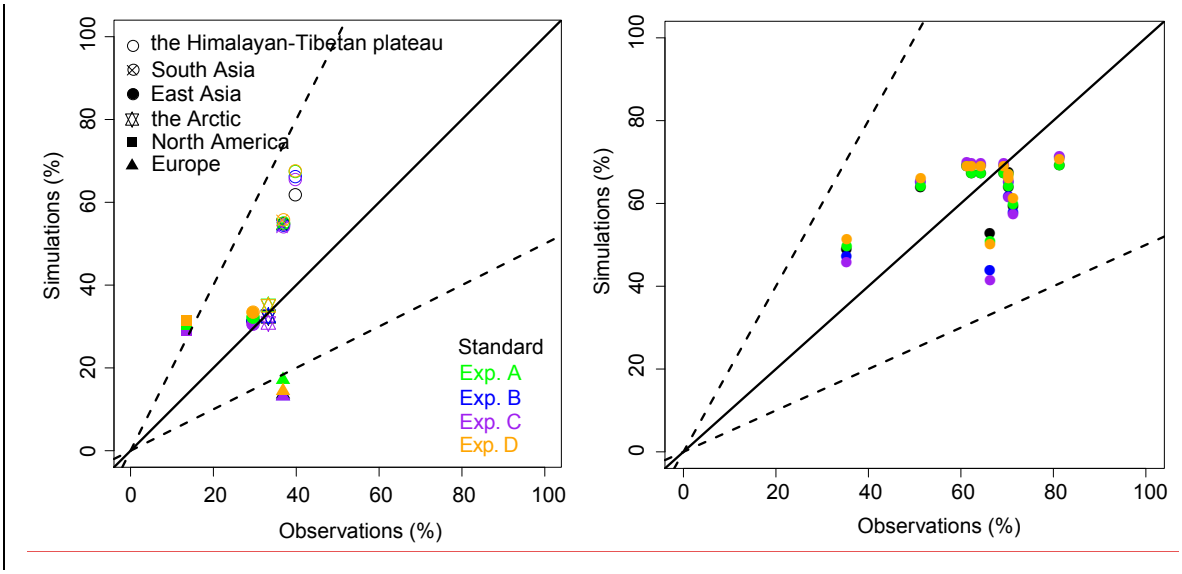

Figure S8. Observed and GEOS-Chem simulated mean f_{bb} (%) (a) of BC in the atmosphere in the six regions in Northern Hemisphere and (b) of BC deposited in snow over the Tibetan plateau. The regions are symbol-coded and the simulations are color-coded (see text for details). Solid lines are 1:1 and dashed lines are 1:2 (or 2:1).